UNIVERSIDADE DE LISBOA

FACULDADE DE CIÊNCIAS

Departamento de Biologia Animal

The Dynamics of Fibroblasts/ECM in Neonatal Cardiac Injury

Vasco Miguel Sampaio Pinto

Dissertação

Mestrado em Biologia Evolutiva e do Desenvolvimento

2014

UNIVERSIDADE DE LISBOA

FACULDADE DE CIÊNCIAS

Departamento de Biologia Animal

The Dynamics of Fibroblasts/ECM in Neonatal Cardiac Injury

Vasco Miguel Sampaio Pinto

Dissertação Orientada pela Doutora Diana Nascimento (INEB) e

Orientador Interno: Professora Doutora Gabriela Rodrigues (CBA/FCUL)

Mestrado em Biologia Evolutiva e do Desenvolvimento

2014

"If you would be a real seeker after truth, it is necessary that at least once in your life you doubt, as far as possible, all things."

René Descartes

1. ACKNOWLEDGEMENTS

Firstly, I want to express my gratitude to Perpétua for the opportunity to work in her team, for her scientific guidance and especially for the welcoming environment so deeply-rooted in the team. I will always consider you my co-supervisor although officially I was not allowed to have one.

Secondly I want to thank Diana for accepting me as her master student, for her attention, dedication and friendship. I want to recognize her for helping me grow as a scientist and also as a person! Moreover I want to thank her for giving me the opportunity to continue to be part of this project at her side.

I want to highlight Gabriela Rodrigues for accepting to be my internal supervisor and for being always available to discuss and for advising me.

I also want to acknowledge all the members of the Stem-cell microenvironments in repair/regeneration team. Tatiana for your sympathy and scientific guidance. Ana Freire for being essentially my second older sister. Mariana for all the help in the lab, namely with histology and flow cytometry. Aninhas for teaching me from very beginning and by all the advices. Tiago for the support and help with the confocal microscopy and for not allowing me to be the only guy in the team.

I am grateful to Catarina Leitão and to André Maia for the help in flow cytometry and in high content screening, respectively. I want to thank all the personnel of the animal facility. Your excellent work is essential for keeping ours running.

Additionally I want to emphasize developmental biology group, namely Sólveig Throsteinsdóttir and Andreia Nunes by helping me during the time I have spent working in Lisbon. Your expertise has been essential for this work.

I want to show gratitude to all the members of the zebrafish office and sea urchin lab by welcoming me so well.

To all Inebian family I want to express my gratitude for allowing me to be part of You!

Aos animais da quinta quero agradecer por me integrarem tão bem e por me levarem a conhecer o Porto e à equipa de futebol por também facilitar essa integração.

Finalmente, mas não menos importante quero agradecer à minha família por todo o apoio que me dá. À Cátia e à sua família quero também agradecer por me terem acompanhado mais proximamente este ano e por facilitarem esta caminhada. Um muito obrigado a todos!

2. ABSTRACT

Cardiac diseases remain the major cause of morbidity and mortality worldwide. This is the ground for an increasing number of studies on the characterization of the heart's response to injury and on the development of new therapies to functionally restore the damaged myocardium. Recently, several reports show that the mammalian heart, when injured in a short-period after birth, displays the capacity to regenerate, whereas, if injured after post-natal day (P)7, it triggers the formation of a non-functional fibrotic scar. However, the signals that determine the development of a reparative (adult) or regenerative response (neonate) are largely unknown. The premise of our Team is that the transient regenerative capacity of the heart is related to specific organ changes during this ontogenic period. The herein work focuses on the dynamics of cardiac fibroblasts and that of the extracellular matrix (ECM) during ontogeny and following injury in the neonate. We demonstrate that fibroblasts, here defined as the $CD31^{-}CD45^{-}Ter119^{-}CD90^{+}$ population, colonize the heart following birth and also that the cell-surface signature of this compartment changes throughout post-natal life. Our results demonstrate that the neonatal heart response to apex resection involves the recruitment of inflammatory cells, fibroblast activation, ECM production and neo-vascularization. High Content Analysis (HCA) revealed that the removed tissue was, at least in part, re-established by the proliferation of resident cardiomyocytes. Moreover, despite formation of scarring tissue (inner core of the injured area) and incomplete histological restoration, resected hearts were functionally competent at 21d post-lesion.

Overall this work describes the microenvironmental alterations, with particular emphasis on fibroblasts and ECM, triggered following neonatal apex resection and that culminate on partial restoration of the organ.

Keywords: Cardiac Injury, Cardiac Fibroblasts, Extracellular Matrix

3. SUMÁRIO

As doenças cardiovasculares são a principal causa de morte nos países de alto e médio rendimento. O transplante cardíaco é o único tratamento eficiente a longo prazo, no entanto, este é limitado pela baixa disponibilidade de dadores e a necessidade de imunossupressão. Após enfarte do miocárdio, a isquemia resulta em elevada morte celular por falta de oxigénio e nutrientes. Uma vez que o coração adulto é incapaz de restabelecer os cardiomiócitos perdidos, que são a força contráctil do coração, a função sistólica fica diminuída e desenvolve-se tecido cicatricial, como resultado de um processo reparativo, na região afectada pela isquemia. Consoante a extensão de tecido afectado pelo enfarte este pode ser fatal ou conduzir a uma perda progressiva de função.

Contudo, no início do século XXI, vários foram os estudos que demonstraram que os cardiomiócitos proliferam na vida pós-natal, ainda que a uma taxa insuficiente para garantir a plena reconstituição do miocárdio após lesão. Esta evidência conduziu a comunidade cardiovascular a investigar sinais que possam levar ao melhoramento da resposta do coração ao enfarte, nomeadamente estimulando a proliferação de cardiomiócitos. Nesse sentido vários modelos animais foram estudados e constatou-se que o peixe-zebra (*Danio rerio*), o axolote (*Amblystoma mexicanum*) e o tritão (*Notophthalmus viridescens*) são capazes de recuperar histo-funcionalmente de lesões cardíacas induzidas experimentalmente, como é exemplo a remoção do ápice cardíaco. Embora estes estudos constituam a primeira evidência de que o coração tem potencial regenerativo, a longa distância filogenética entre estes animais e os mamíferos, questiona o potencial translacional destes estudos.

Surpreendentemente, em 2011, Porrello *et al.* demonstraram que o murganho (*Mus musculus*) detém uma capacidade de regeneração cardíaca transiente, já que esta parece cessar após a primeira semana de vida. Após remoção do ápice em animais no primeiro dia de vida os autores reportam que o coração é restaurado com fidelidade a nível histo funcional. Contudo, quando a mesma lesão é praticada em animais após a primeira semana de vida verificava-se a formação de uma cicatriz fibrótica não funcional, semelhante à formada no órgão adulto após enfarte do miocárdio. Este estudo revolucionou a área cardiovascular uma vez que se considera que este é um modelo útil na identificação de factores importantes para melhorar o processo de reparação do coração adulto humano.

Durante a realização deste trabalho, todavia, Andersen *et al.* (2014) refutaram a existência de regeneração cardíaca em murganho. Os autores verificaram que após remoção do ápice cardíaco há activação de uma resposta inflamatória exuberante, formação de uma cicatriz fibrótica e que os corações eram sistematicamente mais pequenos e apresentavam menor proliferação e vascularização que os respectivos controlos cirúrgicos. Estes resultados instalaram na comunidade cardiovascular uma atmosfera de incerteza quanto à reprodutibilidade do modelo de lesão neonatal e à capacidade regenerativa dos murganhos neonatais.

O coração é composto por vários tipos celulares, nos quais se incluem os cardiomiócitos, elementos vasculares (células do músculo liso e endoteliais) e fibroblastos cardíacos. Atendendo à sua elevada frequência no estroma cardíaco, o papel dos fibroblastos cardíacos foi

rigorosamente avaliado durante o normal funcionamento do coração e em resposta ao enfarte do miocárdio. Apesar da ausência de marcadores fidedignos deste tipo celular, uma vez que ainda não foi descrita uma assinatura molecular própria, sabe-se que estas células são essenciais para a preservação das propriedades físico-químicas do coração, sendo mesmo as principais responsáveis pela produção e secreção da matriz extracelular (ECM) cardíaca. Os fibroblastos cardíacos são também produtores de metaloproteinases (MMPs) que degradam a ECM e, como tal, este tipo celular é responsável por modelar a composição da matriz, o que por sua vez condiciona o comportamento das células aí residentes. Após enfarte do miocárdio, os fibroblastos cardíacos migram para o local da lesão, proliferam e diferenciam em miofibroblastos, os quais expressam ativamente marcadores de músculo liso e depositam colagénio tipo I e III, na região da lesão, gerando uma cicatriz fibrótica não funcional.

Embora se conheça o papel dos fibroblastos cardíacos na lesão do coração adulto, o seu papel na lesão neonatal é totalmente desconhecido. A premissa da equipa *Stem Cell Microenvironments is Repair/Regeneration* do INEB é de que o carácter transiente da regeneração cardíaca resulta de alterações no coração quer ao nível da ECM quer ao nível celular durante a ontogenia do órgão.

Neste trabalho, definimos como objectivos a avaliação da dinâmica da população de fibroblastos cardíacos e da produção de ECM ao longo do desenvolvimento e maturação do coração, bem como durante a resposta à remoção do ápice cardíaco. Usando esta estratégia pretendemos investigar se são apresentados/emitidos sinais pela ECM ou pelos fibroblastos cardíacos, que promovam a proliferação ou maturação de cardiomiócitos. Através do estabelecimento do modelo de ressecção do ápice cardíaco e caracterização histo-funcional do mesmo procuramos providenciar dados empíricos que permitam clarificar se ocorre efectivamente activação de processos regenerativos em resposta à lesão, nomeadamente processos de proliferação de cardiomiócitos.

Contrariamente ao que foi descrito no trabalho pioneiro de Porrello, nas nossas condições, não foi observada a recuperação completa do ápice cardíaco até 60 dias após-cirurgia. Ao invés, detectou-se deposição de uma cicatriz fibrótica composta por colagénio, na zona central de lesão, ainda que sem impacto detectado na função cardíaca.

As variações da componente celular e extracelular durante a lesão foram avaliadas através da co-detecção de marcadores celulares com proteínas da ECM. Imediatamente após a lesão foi possível observar uma disrupção dos padrões de expressão da α-actinina sarcomérica e das proteínas da lâmina basal colagénio IV e laminina na zona de lesão, padrões estes que foram parcialmente restabelecidos aos 21 dias após a lesão. Durante os primeiros 5 dias verificou-se uma forte resposta inflamatória, caracterizada por um elevado número de células hematopoiéticas. Todavia aos 7 dias após-lesão o número de células hematopoiéticas decresce significativamente e acentua-se a presença de fibroblastos e miofibroblastos. A expressão de fibronectina e tenascina-C no local de lesão parece inicialmente estar associada ao coágulo sanguíneo e às células hematopoiéticas, no entanto a partir dos 7 dias pós-cirúrgicos, a sua produção passa a ser assegurada pelos fibroblastos/miofibroblastos. Conseguimos eficazmente correlacionar a expressão de fibronectina e tenascina-C com a proliferação/mitose celular, uma vez que é nos locais onde estas proteínas abundam que há maior expressão de PH3. A análise quantitativa do número de células mitóticas permitiu identificar um maior número de células em mitose e mais especificamente de cardiomiócitos, em corações sujeitos a lesão.

Uma vez que observámos activação e diferenciação de fibroblastos em miofibroblastos após lesão, decidimos estudar o perfil destas células em maior detalhe. Como nunca foi reportada a caracterização de fibroblastos no período pós-natal, avaliámos o perfil de expressão dos fibroblastos, identificados com base na expressão de CD90, ao longo da ontogenia bem como num cenário de lesão. Os fibroblastos cardíacos instalam-se no miocárdio após-nascimento, de forma a constituírem cerca de 60% da população estromal do coração adulto. Adicionalmente, o perfil da população proliferativa no adulto parece ser na sua maioria composto por fibroblastos. Avaliámos a expressão de diferentes marcadores envolvidos na adesão celular e de afiliação mesenquimal na população de fibroblastos, o que salientou a heterogeneidade desta população e alterações do perfil de expressão dos diferentes marcadores ao longo da ontogenia. De salientar é a população Sca-1^{+}, que aumenta de um nível residual a P2 para mais de 70% dos fibroblastos cardíacos (CD90^{+}) no coração adulto.

A população de fibroblastos cardíacos activados pela lesão é constituída maioritariamente por células Sca-1^{+} e CD44^{+}, verificando-se ainda uma redução significativa da expressão de CD29 e de CD140a após lesão. No entanto, considerando o compartimento proliferativo, apenas se verificou-se um aumento na população Sca-1^{+}.

Em suma, demonstrou-se que a resposta do neonatal (P2) à lesão envolve a formação de um coágulo sanguíneo, recrutamento de células inflamatórias, proliferação de miofibroblastos, rearranjo da matriz extracelular e activação da proliferação de cardiomiócitos. A população de fibroblastos cardíacos surge como altamente heterogénea apresentando-se diferente consoante o período ontogénico e em resposta à lesão. A relevância funcional das alterações observadas após lesão e durante a ontogenia requerem investigação futura.

Palavras-Chave: Regeneração Cardíaca, Fibroblastos Cardíacos, Matriz Extracelular

4. CONTENTS

5. INTRODUCTION

5.1. Epidemiology of Cardiovascular Diseases

Ischaemic heart diseases are, according to the World Health Organization (WHO), the leading cause of death worldwide (Figure 1). Despite contribution of genetic factors for development of cardiac pathologies, most risk factors are behaviourally and environmentally linked, such as: age, sex, high blood pressure, hypercholesterolemia, smoking, obesity, alcohol consumption (1); and therefore cardiomyopathies are more frequent in middle and higher income countries. However, the incidence of ischemic heart diseases is also increasing in developing countries mainly due to atherosclerosis-related illnesses (2).

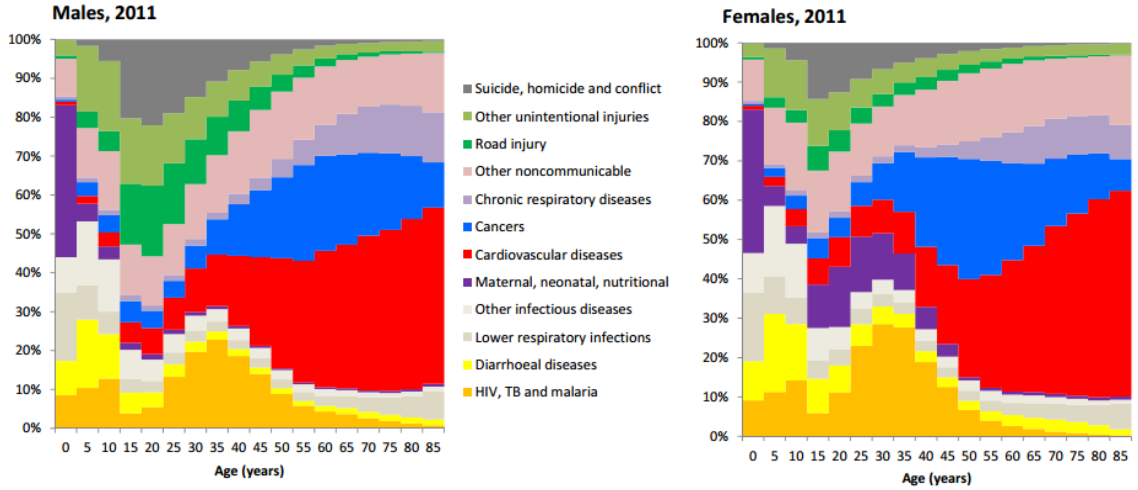

Figure 1 *- Percentage of deathsgrouped by cause for global age-sex groups in 2011. Adapted from (1).*

The only long-term effective treatment for heart failure is heart transplant, which is limited by the shortage of donors (3), organ rejection/failure and side effects related to immunosuppression (4). This scarcity of therapeutic alternatives has propelled the scientific community to question the hypothesis that the working myocardium is a post-mitotic tissue and to investigate new biological scenarios in which the heart demonstrates regenerative potential.

For many years, the view of the heart as a post-mitotic organ has been considered the main reason for the myocardial inability to histo-functional restoration following myocardial infarction (MI), forming, instead, a non-functional fibrotic scar, as a culmination of a reparative response. However, by the turn of the century, several studies demonstrated that cardiomyocytes renew during post-natal life. This observation first came from injured hearts. According to Beltrami and colleagues, hearts that undergone MI exhibit 70 times more cardiomyocyte proliferation in the border zone when compared to healthy hearts and 24 times more cardiomyocyte proliferation in distant myocardium (5). Taking advantage of Carbon-14 integration into DNA, during Cold-War nuclear tests, Bergmann *et al.* estimated that, in non-manipulated conditions at the age of 25, annual cardiac turnover is around 1% and that this percentage is reduced to 0.45% at the age of 75 (6). The revelation that cardiomyocytes, the heart's working force, could renew both in healthy and in injury conditions, was the proof of concept that the heart endows an intrinsic potential that can be potentially optimized in an injury scenario. In the years that followed, cardiovascular community focused mainly on the origin of newly-formed cardiomyocytes. Two contrasting ideas gradually developed: one

claiming that cardiomyocytes originate by the differentiation of myocardium-resident cardiac progenitor cells (CPCs), a multipotent cell-type, also able to give rise to endothelial and smooth muscle cells, which are scarcely interspersed in the myocardium (7, 8). Alternatively, others have proposed that the majority of newly formed cardiomyocytes arise from the proliferation of pre-existing cardiomyocytes by cell cycle re-entry (5, 6, 9).

CPCs have been recognized by expression of different cell membrane markers, *i.e.* c-Kit, Sca-1, Abcg-2 and PDGFR-α, and several transcription factors (e.g. *Isl-1*; *Nkx2.5*; *Gata4* and *Wt-1*) (10). Yet, a universal marker of CPCs is still to be identified (11). Recently, it was demonstrated that after selective ablation of c-Kit expressing cells, the restoration of the damaged myocardium was halted, being resumed after the replacement of the ablated CPCs with the progeny of one c-Kit expressing cell (8). This suggested that c-Kit$^+$ cells are necessary and sufficient for myocardial repair. In fact, Stem Cell Infusion in Patients with cardiOmyopathy (SCIPIO) clinical trial have shown a significant improvement of the left ventricle ejection fraction in infarcted patients (12). A different human clinical trial, based in Sca-1 expressing cells, named CArdiosphere-Derived aUtologous stem Cells to reverse ventricular dySfunction (CADUCEUS), demonstrated to improve the health status of myocardial infarcted patients mainly due to an increase of the viable myocardium and decrease in the scar formation (13).

Despite the existence of empirical data supporting each hypothesis, it is yet unclear, which is the most prominent source of new cardiomyocytes. However, and regardless the adopted premises, it is unanimously accepted that cardiomyocyte renewal is insufficient to assure functional restoration of the adult heart following MI. Hence, biomedical cardiovascular community is actively engaged in the development of therapeutic alternatives that envisage the generation of new cardiomyocytes in adequate numbers to re-establish the contractile capacity of the damaged heart.

5.2. The Phylogenetic Axis of Cardiac Regeneration

Regeneration, the ability to restore a lost body part, is a common phenomenon, widely disseminated in metazoans, that can occur at different biological levels (14) (Figure 2).

In a broad perspective regeneration occurs by the *de novo* synthesis of functional tissue through recapitulation, to a varying extent, of the embryonic program that gave rise to the original tissue (15). Numerous efforts have been employed to identify similarities between regenerative responses observed in several animal models, aiming at targeting the molecular and biological players transversal to such phenomena (16). The comparison of embryonic (scar-free healing) and adult (scar-formation) response to skin wounds allowed Ferguson and colleagues to determine the levels of morphogens present in scar-free conditions. More impressively, restitution of those levels in adults, preceding injury, resulted in scar-free wound healing resembling the embryonic response (17).

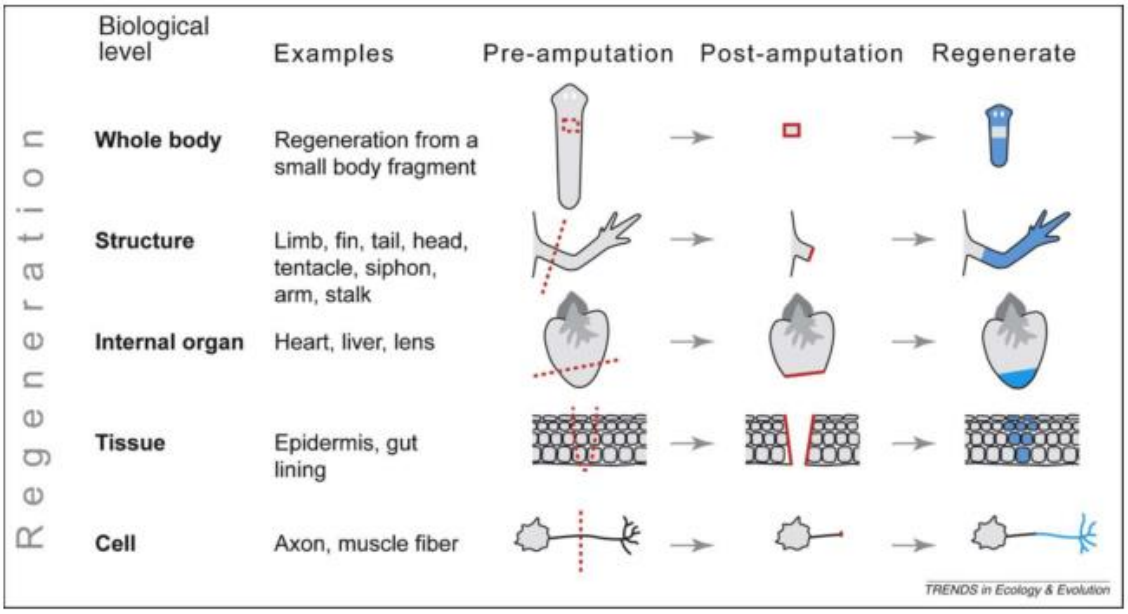

Figure 2 – *Biological organization of regeneration. Adapted from* (14).

Apart from the planarian (*Planaria sp.*), that has the extraordinary ability of regenerate entire organisms from tissue fragments (18), the most conspicuous evidence of regeneration is the restoration of whole body parts, often lost due to sublethal predation, the most common cause of tissue loss in nature (14). In vertebrates, whole-body regeneration is exclusive of amphibians, reptiles and fish, and therefore model-systems representative of these animal classes have been the subject of numerous studies regarding regeneration. In fact, the first evidence of heart regeneration was demonstrated in zebrafish (*Danio rerio*). After surgically resecting 10 to 20% of the adult ventricle myocardium in the apex region, the heart progressively restores the lost tissue within 60 days (19). Initially a blood clot is formed which is gradually replaced by newly formed cardiomyocytes, restoring the contractility to the original levels. Cre-Lox transgenic zebrafish have provided additional evidence that the regenerative response encompasses dedifferentiation and proliferation of pre-existing cardiomyocytes (20).

Recently, cardiac regenerative potential of zebrafish was further demonstrated in different injury models. Cryoinjury of the ventricle was used to test whether zebrafish hearts would also recover from ventricular necrotic lesions. In fact, complete heart recovery by means of cardiomyocyte proliferation and invasion to the injury site was revealed (21). Concordantly, after genetic depletion of more than 60% of the ventricular myocardium, due to the induction of diphtheria toxin A chain (DTA) expression in cardiomyocytes, zebrafish hearts are still able to recover within several days by cardiomyocyte proliferation (22).

Urodele amphibians, which include newts and salamanders, also display heart regeneration upon cardiac injury. Alike zebrafish pioneering work, after surgical resection of the ventricle apex of axolotl *Amblystoma mexicanum*, a blood clot is formed to prevent an extensive blood loss, followed by the establishment of a strong inflammatory response that is reduced overtime while tissue recovery is achieved by cell-cycle re-entry of pre-existing cardiomyocytes (23). The cardiac regenerative capacity of urodeles was further confirmed by applying a different injury model to newts while obtaining a similar regenerative response (24).

Evidence that the mammalian heart might also display a regenerative injury response was demonstrated in 2011 by Sadek's team, using the mouse as a model-system. Contrarily to lower vertebrates, murine cardiac regenerative response was described as transient given that after surgical apex resection in 1 day old animals (P1), hearts progressively restored the lost tissue, however, when the same procedure was performed at P7, hearts did not recover and developed significant fibrosis (Figure 3). Hence, while the heart's injury response at P1 is characterized by proliferation of pre-existing cardiomyocytes, response at P7 resembles the reparative response of adult mammals to MI, i.e. formation of a fibrotic non-functional scar (25).

In addition to the apex-resection model, the same group and an independent group established the neonatal MI model, thus confirming that the mammalian heart could also regenerate, in a ischemic senario (26–28). P1 mice were subjected to MI by ligation of the left descending coronary arthery. This procedure induced extensive myocardial necrosis and systole dysfunction. However, faitfully to the apex-resection model, the heart was able to fully recover within 21 days by proliferation of the preexisting cardiomyocytes (28, 29). More importantly, the authors came forward with a mechanistic explanation for the very low rates of proliferating cardiomyocytes and subsequently to the loss of cardiac regeration from P7 onwards. The inhibition of miR-15 family of microRNAs, from an early postnatal age until adulthood, augments the number of proliferating cardiomyocytes in the adult heart and to an improvement on left ventricular systolic function of adult myocardial infarcted hearts (26, 29), therefore implicating this microRNAsin the neonatal loss of cardiac regenerative capacity.

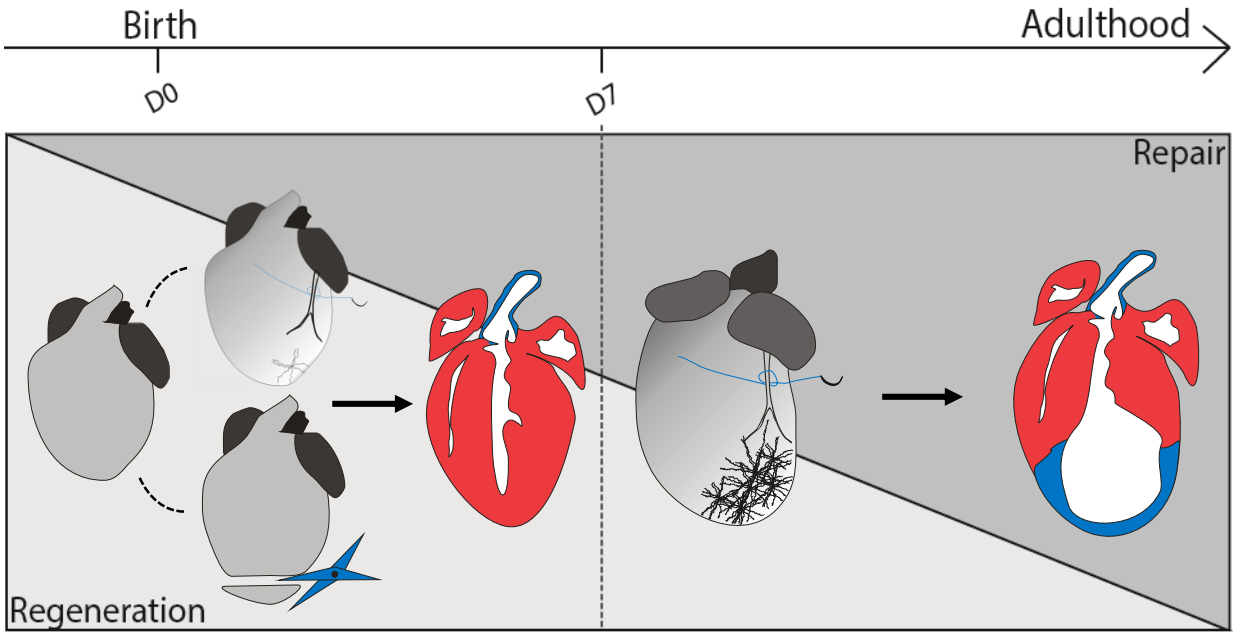

***Figure 3** – Schematic representation of the ontogenic-specific heart-response to injury, characterized by main predominance of regeneration in the first post-natal week (regardless of the used injury model) in contrast to the well-reported reparative response of the adult heart to injury*

Despite evident phylogenetic distance between mammals, fish and amphibians, the main hallmarks of the heart regenerative course seem to be conserved, namely the formation of a blood clot and establishment of a strong inflammatory response, which are gradually replaced by newly contractile myocardium, arising from pre-existing cardiomyocytes.

Curiously, the loss of cardiac regeneration in neonatal mice coincides with physiological cardiomyocyte maturation that occurs post-birth. In fact, at this timeframe, i.e. in the first week post-birth, there is a switch from hyperplasic to hypertrophic growth concomitant with cardiomyocyte binucleation (in rodents) (30).

Recently, close association between immune response and mammalian cardiac regeneration has been demonstrated. First, the inflammatory response is of great relevance given the necessity to remove cell debris. Furthermore, macrophages and other immune cells produce soluble factors that may influence other cell types. In fact, macrophages from regenerative (P1) and reparative (P14) hearts exhibit different molecular signatures, e.g. P1 macrophages express pro-angiogenic cytokines, which are crucial for successful tissue restoration. More impressively, neonatal regenerative response is halted following specific macrophages ablation (31) and thus rendering the immune modulation as a novel objective for newly developed clinical alternatives.

5.3. The Downfall of the Paradigm

Since Sadek's team breakthrough, neonatal regenerative capacity of the mouse heart has been fully accepted and established, as such that his work has been cited over 200 times.

However, in 2014 and therefore during the realization of this work, the controversy was settled when Andersen *et al.*, while attempting to establish the neonatal heart injury in an inbred mouse strain, obtained and reported no evidence of complete regeneration (32). These authors documented a strong inflammatory response in the injury site, followed by massive collagen deposition. Additionally, resected hearts were shown to be smaller and with reduced cardiomyocytic proliferation and vascularization when compared to sham-operated controls. This deceptive outcome has created doubts concerning the reproducibility of the neonatal injury model and on the ability of neonates to regenerate their hearts. In our perspective the concept of "complete regeneration" is rather unclear, so more important that the idea of neonatal full-apex restoration is the ability of neonates to respond to injury by reactivation of neomyogenic mechanisms. In line with this, it is crucial to clarify whether this is an appropriate model to dissect mechanistic aspects underlying the activation and proliferation of cardiomyocytes that can be relevant for the implementation of therapeutic alternatives for adult-heart repair.

5.4. The role of Cardiac Fibroblasts and of Extracellular Matrix in Response to Injury

The heart is a complex organ, composed by several cell types, which include: cardiomyocytes; vascular elements (e.g. smooth muscle and endothelial cells) and cardiac fibroblasts (33). Indeed, although cardiomyocytes occupy the majority of heart's volume, the most common cell type are cardiac fibroblasts (34, 35). The specific contribution of each cardiac cell, as well as of their interstitial surroundings, i.e. extracellular matrix (ECM), to the injury response observed in the neonatal heart is yet to be determined.

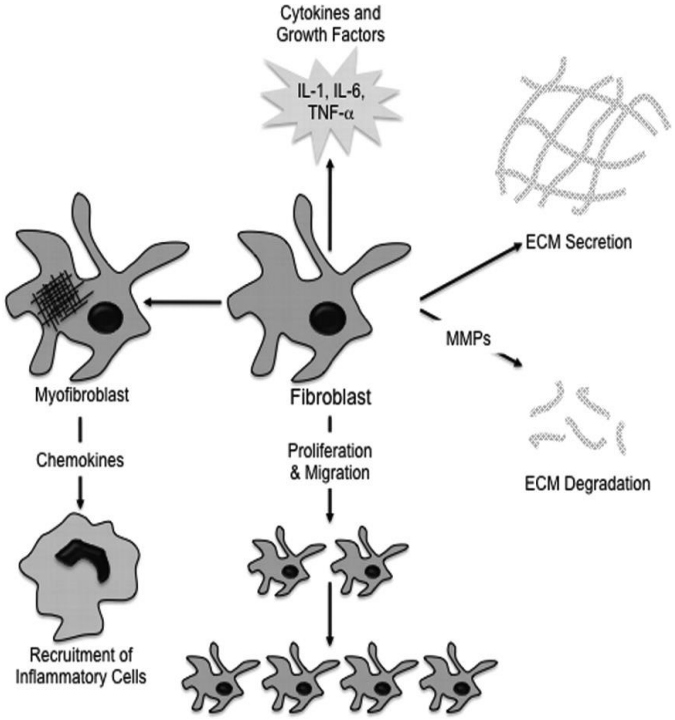

Figure 4 – *The diversity of functions of cardiac fibroblasts in response to myocardial infarction. Cardiac fibroblasts mediate injury response either through secretion of paracrine factors, differentiation into myofibroblasts and ECM modulation. Adapted from [19].*

Cardiac fibroblasts and fibroblasts, in general, have been considered the main producers of ECM. In addition cardiac fibroblasts also produce and secrete metalloproteinases (MMPs) that are responsible for ECM degradation. Importantly, the dynamic equilibrium of the ECM composition modulates the behaviour of neighbouring cells (36, 37).

The role of cardiac fibroblasts in heart remodelling following MI has been meticulously scrutinized (Figure 4).

Scarcity of oxygen and nutrients inherent to myocardial ischemia leads to massive cell dead and, in turn, necrotic/apoptotic cells release dead signals, which recruit immune cells to the injury site (38). Hence, after ligation of the left anterior descending coronary artery of adult mice, infiltration of neutrophils/macrophages is evident within the first 4 days (39).

Along with inflammatory cells, cardiac fibroblasts migrate to the damaged tissue and proliferate massively and a fraction differentiates into myofibroblasts. These are recognizable by expression of smooth muscle cell markers, such as α-smooth muscle actin (αSMA) and by displaying spontaneous contractions, which are thought to be involved in appropriate wound closure and structural integrity of healing scars (40). These cells have a direct role in the recruitment of newly inflammatory cells to the damaged tissues through chemokine secretion (33). Myofibroblasts and fibrosis have been classically associated (41) since this cell type and also resident fibroblasts are responsible for abundant secretion of collagen type I and III in the injury site (42). The accumulation of collagen is the foundation of a stiffer and dense ECM, also known as fibrotic scar, which is completed within 21 days post-MI. (37, 39, 43).

Indeed, the development of a fibrotic scar constitutes a quick and efficient response to trauma in the sense that is responsible for structurally supporting the compromised heart. Notwithstanding, once it is non-functional, as it is virtually stripped of cardiomyocytes, cardiac function is significantly affected.

The role of cardiac fibroblasts in neonatal cardiac injury has never been ascribed. The transient nature of the regenerative response can be explained by fluctuations in the population of resident cardiac fibroblasts after birth. Nevertheless, several lines of evidence suggest that fibroblasts may be a key player in this process. Indeed, following birth cardiac ECM suffers a major transition in terms of biochemical composition that impacts on the heart´s mechanical properties (in detail in Section 5.). These alterations suggest post-natal phenotypic alterations

on the fibroblast population/s. Our working premise is that the latter may have a direct impact on cardiomyocytes behaviour, imposing a swift on cardiomyocyte phenotype from hyperplasic to hypertrophic growth. In fact, immature embryonic cardiac fibroblasts were shown to induce cardiomyocyte proliferation via β1-integrin signalling, whereas mature adult cardiac fibroblasts enhanced cardiomyocyte maturation, namely by stimulating hypertrophy (36).

The main limitation of studying cardiac fibroblasts is the absence of a reliable fibroblast marker. Although some proteins, e.g. fibroblast specific protein 1 (FSP1) (44), periostin (45), discoidin receptor domain 2 (DDR-2) (46), transcription factor 21 (TCF-21) (47), CD90 (Thy-1) (48) have been used for prospective identification of fibroblasts, there are several advantages and limitations associated with each marker, which highlights the need of carefully reviewing the conclusions drawn by their usage.

The ECM is currently defined as the extracellular portion of a multicellular structure that provides structural and biomechanical support to cells. ECM can be divided into two categories: the basement membrane and stromal/interstitial matrix. The first consists in a thin layer of molecules that surround and support cells and bridges the cellular compartment with the respective stromal matrix. Once it is this type of matrix that is in touch with cells, it is this subtype that has more impact on cell behaviour and function (49). The stromal matrix is responsible for the main tissue structural support due to the large amount of fibrous molecules in its composition (50).

The ECM is recognized as a bioactive unit that modulates neighbouring cell behaviour either directly, by cell-matrix interactions mediated by integrins, or indirectly, by paracrine effects of molecules sequestered in the ECM network (51). Additionally, ECM is a dynamic structure that is affected by microenvironmental stimuli, such as during development and following tissue injury, by adjusting the composition, stiffness, organization and, ultimately, the function. ECM plasticity certainly accounts for the fact that ECM is critical for organ formation and repair, which has been recognized for a long time (52, 53).

The cardiac ECM is composed by several different types of molecules, including different types of collagen, a variety of glycoproteins and proteoglycans. Cardiac fibroblasts and vascular smooth muscle cells are responsible for the production of the most common cardiac ECM proteins such as collagen I and III. In turn, cardiomyocytes produce essentially the proteins present in their basal lamina (e.g. collagen IV and VI, laminin and proteoglycans) (54, 55). However, after birth there is a significant decrease on the levels of fibronectin and elastin (56) and also a dramatic change in the elastic modulus of epicardium following birth from 12 kPa to 39kPa (57). Consistently, during aging the levels of collagens are enriched (58). This correlates with a decrease in the myocardial elasticity, compromising to a limited extent, the cardiac function (59). In our perspective these changes throughout ontogeny, and specifically after birth, may be determinant to the transition between regenerative and reparative behaviour of the heart.

In fact, several evidences demonstrate that ECM is essential for the regenerative response generated upon cardiac injury. Following apex-resection of adult zebrafish, epicardial cells dynamically produce fibronectin. Concomitantly, cardiomyocytes augment the levels of α5 and β3 integrins that are constituents of fibronectin receptors, which leads to specific triggering of integrin signalling pathways and cardiomyocyte proliferation and migration (60). Moreover, the

authors, by using a transgenic line that enables a heat-inducible expression of a dominant-negative human fibronectin fragment, showed that in the absence of fibronectin no regeneration was observed.

Notwithstanding, transforming growth factor-β (TGF-β) ligand and receptors, which are induced in fibroblasts and cardiomyocytes following cryoinjury, are also required for heart regeneration in zebrafish (Figure 5).

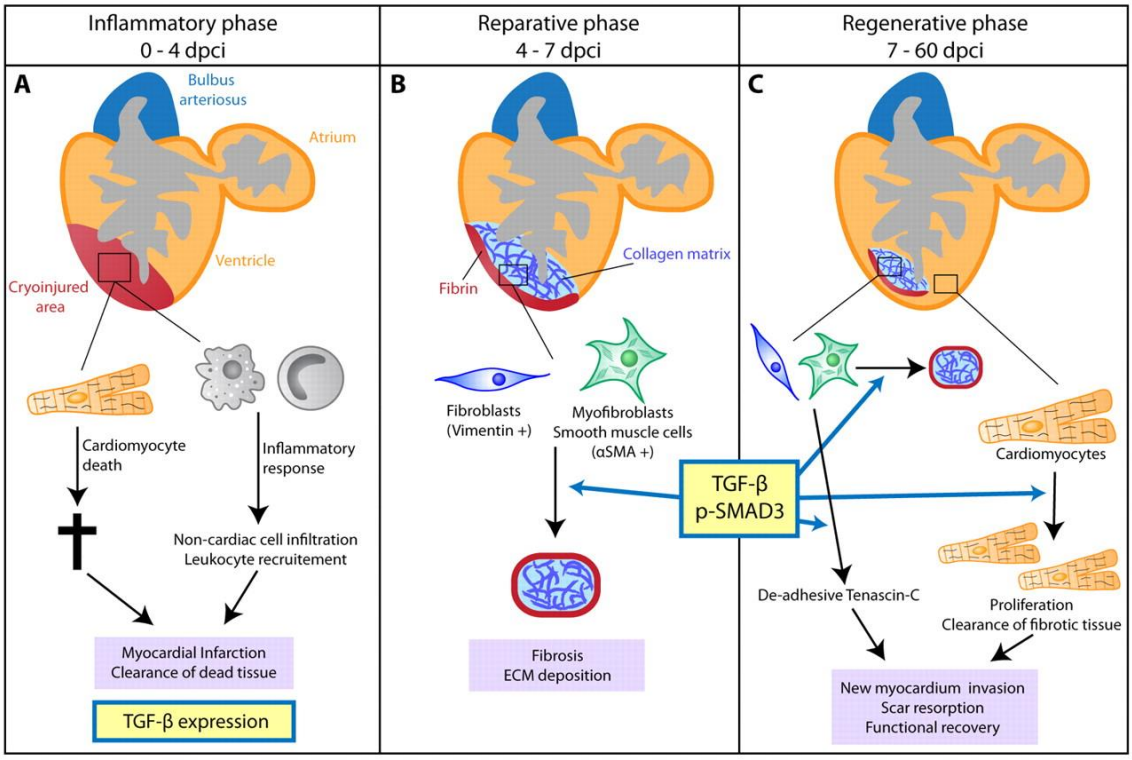

Figure 5 – *The role of TGF-β signalling pathway in zebrafish heart response to cryoinjury. Cardiomyocyte death leads to an inflammatory response and migration of leukocytes and fibroblast-like cells actively expressing TGF β (A). Once the majority of death tissue is cleared, a TGF-β signalling-mediated collagen-rich extracellular matrix is formed (B). As scaring begins TGF-β induces the proliferation of neighbouring cardiomyocytes that migrate to the injured area, replacing the fibrotic scar (C). Cardiomyocytic proliferation seems to be Tenascin-C dependent, mainly due to its anti-adhesive properties(61)(61)(61)(61)(61)(61)(61)(61)(61)(61)(61)(61)(61)(61)(61). Adapted from* (61)

A recent study in the adult newt (*Notophthalmus viridescens*) demonstrated that, following apex-resection tenascin-C, hyaluronic acid and fibronectin are up-regulated, which precedes the proliferation and migration of cardiomyocytes to the injured area. In order to address whether these ECM components were having an instructive role in cardiomyocytes, primary newt cardiomyocytes were plated on regeneration-specific ECMs. In fact, cardiomyocytes displayed the highest proliferation levels in the presence of Tenascin-C, suggesting that this protein is directly or indirectly promoting cardiomyocyte proliferation (62).

The herein MSc dissertation will evaluate the dynamics of cardiac ECM and its main producer, the cardiac fibroblast, during regenerative and reparative ontogenic stages as well as in response to neonatal heart injury. We anticipate that fibroblast/ECM-specific regulators of cardiomyocyte proliferation/maturation will be identified which may hold great potential for treatment of cardiac pathologies associated with cardiomyocyte loss. Moreover, by independently establishing the neonatal apex-resection injury model we expect to provide empirical evidence aiming at clarify whether there is indeed activation of regenerative processes in the neonatal

murine heart following apex-resection, namely through the reactivation of cardiomyocyte proliferation.

6. Methods

6.1. Animals

All animal experiments were performed in accordance with IBMC.INEB Animal Ethics Committee and to DGAV. Humane endpoints were performed in accordance with the OECD Guidance Document on the Recognition, Assessment, and Use of Clinical Signs as Humane Endpoints for Experimental Animals Used in Safety Evaluation (2000). C57BL/6 mice from embryonic day (E)17 to 8 weeks were used in this study.

6.2. Neonatal Apex-Resection and Sham-Surgery

The neonatal injury model consists in apex surgical resection of post-natal day (P)2 C57BL/6 mice. Animals were anesthetized by hypothermia during approximately three to four minutes to cease respiratory movements and heart contractions and lose the paw withdrawal reflex. Animals were laid in lateral decubitus position, exposing the left-side flank. After animal immobilization with sealing tape, the skin was cut and muscle fibres disrupted until ribs were observed. The thoracic cavity was opened in the 4th intervertebral space and the left ventricle apex cut with fine scissors. The thorax was closed by 6-0 absorbable suture (Coated Vicryl Ethicon) and skin closed by tissue adhesive (3M Ventbond^{TM}). The animal recovered under an infrared lamp and was subjected to stimulation by tightening the paw. The surgery was complete when the animal regained regular breathing. After operating all animals from the same litter, neonates were returned to the progenitor cage given t they rely on the mother for temperature regulation and food. During all the procedure, except throughout surgery, neonates were warmed by warming pads and infrared light. Sham mice underwent the exact same procedure with the exception of apex-resection.

6.3. Histological Analysis

Hearts were harvested at 0, 2, 5, 7, 14, 21 and 62 days post-apex resection (dpr)). Until day 14 the pups were sacrificed by decapitation, using the single movement of a scissor. For longer timepoints, animals were sacrificed by cervical dislocation. Hearts were submersed in phosphate buffer saline (PBS) and fixed in 10% formalin neutral buffer (VWR BDH & Prolabo) either during 24 hours at room temperature or 48 hours at 4ºC. For paraffin embedding, hearts were processed during a total time of 12 hours in an automated system through successive PBS washes, crescent series of alcohols (Aga), Clear Rite 3® (Richard-Allan Scientific) and Shandon Histoplast (Thermo Scientific) at 56ºC. Hearts were included in paraffin and sectioned (microtome RM2255, Leica) longitudinally (3 µm sections). For representative sampling of the heart 10 series of cuts equally distanced were obtained. The distance between sections was specific for each ontogenic stage (0 dpr – 50 µm; 2 dpr – 30 µm; 5 dpr – 100 µm, 7 dpr – 40 µm and 14 dpr – 100 µm; 21 dpr – 70 µm; 62 dpr – 100 µm). Sections were dewaxed and rehydrated prior to Hematoxylin-Eosin (HE) and modified Masson's Trichrome (MT) stains. Briefly, for HE stain, sections were incubated 5 minutes in Gill's Hematoxylin (GHS232, Sigma-Aldrich),

followed by bluing in 0,5% ammonia for 4 seconds or 2 minutes in tap water. Sections were then dehydrated through graded alcohols and incubated for 2 minutes in alcoholic eosin (Leica & Thermo). The MT was performed according to the Trichrome (Masson) Stain kit (HT15-1KT, Sigma-Aldrich), with the following modifications: nuclei were prestained with Celestine Blue solution after staining with Gill's Hematoxylin and incubation for 1 hour in aqueous Bouin solution to promote uniform staining. Sections were diafanized in xylene and mounted in DPX Mountant for histology (06522, Sigma-Aldrich®). Whole-heart images were acquired in a Olympus SZX10 stereomicroscope. High-magnification images were acquired with the inverted fluorescence microscope Axiovert 200 Motorized and an AxioCam HRm camera (Zeiss, Oberkochen, Germany).

6.4. Functional Characterization

Animals at 21 dpr (n=4) were subjected to echocardiography using the Vevo2100 system and a 40MHz probe. Anaesthesia was induced in a chamber filled with 5% isoflurane (IsoVet, Braun). and verified by loss of body posture and paw withdrawal test. The animal was transferred to a 37ºC heated support and the state of anaesthesia was maintained through a face mask (1.5% isoflurane). Animal fur was shaved and mice paws were placed over sensors and in contact with an electric-conductive gel to monitor heart and respiratory rates. The temperature was assessed using a rectal probe. This system assists on the calculation of the heart ventricle wall thickness and the diameter of the ventricular chambers during the diastole (LVIDd) and the systole (LVIDs). These measurements were done to calculate the ejection fraction (EF) and fraction shortening (FS) and thus predict the systolic function of the animal. By comparing these factors on sham operated and injured hearts the degree of functional restoration was ascertained. Two-dimensional (2D) mode images of short-axis (SAX) and parasternal long-axis (PSLAX) were acquired to position the Motion-mode (M-mode) cursor. To evaluate LV structural changes, several parameters from M-mode were measured (that is, the LV internal diameter at diastole (LVIDd) and at systole (LVIDs). Left ventricular ejection fraction (EF) and fraction shortening (FS) were calculated as an index of systolic function: FS (%) = ((LVIDd - LVIDs)/LVIDd) × 100 and EF (%) = $((LVIDd^3 – LVIDs^3)/LVIDd^3) \times 100$. The same parameters were measured on nonmanipulated healthy animals (n =3).

6.5. Immunofluorescence

To further characterize apex-resected and sham-operated hearts by immunofluorescence, these were embedded for cryosectioning. Tissue processing involves 3 consecutive submersions (each during 24 hours at 4^{o}C) in different solutions: 0,2% Paraformaldehyde in 0,12M phosphate buffer; 4% sucrose in 0,12M phosphate buffer and 15% sucrose in 0,12M phosphate buffer. A fourth incubation is performed in 15% sucrose and 7,5% gelatin in 0,12M phosphate buffer with during 1 hour at 37^{o}C. Hearts were transferred to molds containing the last solution (warmed) and placed on top of dry-ice-chilled 2-methylbutane (GPR Rectapur, VWR). Frozen hearts were

stored at -80^{o}C before being cut from one end to the other into 5µm sections using the refrigerated microtome (Microtom HM 550, Thermo Scientific).

Cryosections were used to evaluate protein expression. When targeting epitopes that required cell membrane permeabilization, sections were treated with 0.2% Triton X-100 (for intracytoplasmic motifs) or with 1% Triton X-100 (for nuclear motifs). Tissue sections were blocked for 1 hour in 4% FBS and 1% bovine serum albumine (BSA). If the primary antibody was produced in mouse, the M.O.M.^{TM} Immunodetection Kit (Vector Lab) was applied to enable blocking of endogenous Fc receptors that could be recognized by the secondary antibody (63). Incubation with primary antibody was performed in a humidified chamber 2 hours at room temperature (RT) or, alternatively, overnight at 4ºC. Following the primary antibody incubation sections were incubated with the secondary antibody (RT) during 1 hour. In order to amplify the fluorescence intensity of several antibodies, two streptavidin conjugated fluorophores were used, which were: Streptavidin conjugated with Alexa 555 (S32355, Invitrogen), at 1:500 dilution and Streptavidin conjugated with Allophycocyanin (APC) (SA1005, Life Technologies), at 1:100 dilution. Sections were mounted with Fluoroshield^{TM} with DAPI (F6182, Sigma-Aldrich) and were observed in a Zeiss Axiovert 200M, an inverted fluorescence microscope. Fluorescent images were captured using a monochromatic camera (AxioCam MNC, Carl Zeiss).

Table 1 – *List of primary antibodies used and specification of the working dilution.*

Primary Antibody	Dilution	Reference
Sarcomeric-αActinin (Mouse IgG)	1:400	A7811, Sigma
Tcf21 (Rabbit IgG)	1:100	ABIN1385977, Antibodies-Online
Vimentin (Mouse IgG1/K)	1:50	MS-129-P, Thermo
Vimentin (Mouse IgM)	1:8	40E-C, D.S.H.B.
CD31 (Goat IgG)	1:250	sc-1506, Santa Cruz Biotechnology
CD45 (Goat IgG)	1:100	AF114, R&D
Alpha-Smooth Muscle Actin (Mouse IgG)	1:400	A5228, Sigma
Collagen IV (Goat IgG)	1:50	AB769, Millipore
Collagen IV (Rabbit IgG)	1:100	AB756P, Chemicon
PH3 (Rabbit IgG)	1:250	#3377, Cell Signaling
Fibronectin (Rabbit IgG)	1:400	F-3648, Sigma
Laminin (Rabbit IgG)	1:400	L9393, Sigma-Aldrich
Cleaved Caspase-3 (Rabbit IgG)	1:100	#9661, Cell Signaling
Tenascin (Rat IgG)	1:100	LAT-2, Sonnbg
PLVAP (Rat IgG)	1:8	MECA-32, D.S.H.B.

Table 2 - *List of secondary antibodies used and specification of the working dilution*

Secondary Antibody	Dilution	Reference
Alexa Fluor 488 Donkey anti Mouse IgG	1:1000	A-21202, Invitrogen
Alexa Fluor 568 Donkey anti Rabbit IgG	1:1000	A-10042, Invitrogen
Alexa Fluor 568 Donkey anti Goat IgG	1:1000	A-11057, Invitrogen
Alexa Fluor 488 Goat anti Mouse IgG	1:1000	A11017, Molecular Probes
Alexa Fluor 568 Goat anti Rat IgG	1:1000	A11077, Molecular Probes
Alexa Fluor 633 Goat anti Rabbit IgG	1:1000	A21070, Molecular Probes
Alexa Fluor 488 Donkey anti Rat IgG	1:1000	A-21208, Invitrogen
Biotinylated Donkey anti Goat IgG	1:250	A16009, Life Technologies
Biotinylated Donkey anti Rabbit IgG	1:250	A16033, Life Technologies

6.6. High Content Screening (HCS)

The proliferative response of neonatal murine hearts following injury was evaluated using the GE IN Cell Analyzer 2000. Whole-heart images at 7 dpr and dps were obtained by the assembly of individual pictures at 20x magnification. Using IN Cell Investigator software, the total number of cells was determined (using DAPI as proxy). Mitotic cells were ascertained by the co-localization of DAPI and PH3, whereas mitotic cardiomyocytes by the co-localization of DAPI, PH3 and sarcomeric-αActinin.

6.7. Flow Cytometric profile of Cardiac Populations

Flow cytometry was performed to characterize cardiac fibroblast populations, selected on the basis of CD90 expression, from E17 to adulthood. This characterization was also extended to 7 dpr/dps animals.

Cardiac cells were isolated by digestion of cardiac tissue fragments with crude collagenase (C2139, Sigma-Aldrich®) at 200µg/ml concentration and DNase (A3778, VWR) at 60U/ml in hanks balanced salt solution (HBSS) (H9269, Sigma-Aldrich®). Collagenase digestions were performed during 15 min at 37ºC until no tissue was observed by visual inspection. After each digestion, the suspension was decanted, the media collected (cellular portion) and a new collagenase/DNase solution was added to the remaining tissue fragments. The collected cell suspension was mixed with HBSS with 10% FBS to neutralize enzymatic activity and was kept on ice. The collected cellular fraction of each digestion were combined and washed in FACS medium (0.01% Na-azide 1% FBS in PBS). Cells were evenly distributed for each staining in a round-bottom multiwell plate. After a first wash in FACS buffer, cells were incubated during 25 min with the antibody cocktail on ice and in the dark. In case of biotinylated primary antibodies were

used cells were incubated in the appropriate conjugated streptavidin for 15 min on ice and in the dark. Cells were washed twice in FACS and transferred to FACS tubes

In order to exclude nonviable cells from the analysis, 0.5% of propidium iodide (P4170, Sigma-Aldrich) was added to the cell suspension 1-2 min prior to analysis.

To analyse the nuclear proliferative marker Ki-67, cells were fixed and permeabilized prior to staining according to Foxp3 Staining Buffer Set (00-5521-00, eBiosciences) and Permeabilization Buffer (00-8333, eBiosciences).

Fifty thousand events (of appropriate size and complexity) per staining were acquired in the cytometer FACS Canto II (BD Biosciences). Subsequent analysis and graphing were executed in FlowJo_VX software.

Table 3 – *List of antibodies and streptavidins used in Flow Cytometry and specifications of the working dilution.*

Antibodies	Dilution	Reference
CD31-PE (FL2) (RatIgG2a)	1:100	553373, BD Pharmingen
CD31-PeCy7 (Rat IgG2a)	1:100	25-0311, eBiosciences
CD31-APC (Rat IgG2a)	1:400	102516, Biolegend
CD45-PE (FL2) (Rat IgG1)	1:100	22150456S, Immunotools
CD45-PeCy7 (Rat IgG2b)	1:100	25-0451, eBiosciences
CD45-Biotinylated (Rat IgG2b)	1:500	103103, Biolegend
TER119-PE (Rat IgG2b)	1:100	116208, Biolegend
TER119-PeCy7 (Rat IgG2b)	1:100	116221, Biolegend
TER119-Biotinylated (Rat IgG2b)	1:100	116203, Biolegend
CD90.2-PE (Rat IgG2a)	1:100	553014, BD Pharmingen
CD90.2-FITC (Rat IgG2b)	1:100	553013, BD Pharmingen
CD29-Pacific Blue (Armenian Hamster IgG)	1:100	102224, Biolegend
CD140a-APC (FL4) (Rat IgG2a)	1:100	135907, Biolegend
Flk-1-APC (FL4) (Rat IgG2a)	1:100	560070, BD Pharmingen
Sca-1-PeCy7 (Rat IgG2a)	1:100	108114, Biolegend
Sca-1-FITC (FL1) (RatIgG2a)	1:100	11-5981, eBiosciences
CD44-APC/Cy7 (Rat IgG2b)	1:100	103027, Biolegend
CD105-PE (FL2) Rat IgG2	1:100	120407, Biolegend
CD106-PE (Rat IgG2a)	1:100	105713, Biolegend
CD140b-PE (FL2) (Rat IgG2a)	1:100	12-1402, eBiosciences
Streptavidin-APC	1:800	554067, BD Pharmingen

6.8. Statistical Analysis

Data statistical analysis was performed with the IBM SPSS Statistics 20 software. Shapiro-Wilk's test was used to evaluate if the data displayed a normal distribution. If so, the homoscedasticity of the data was tested by Levene's test. These results defined the statistical test(s) used further. Normal distributed and homocedastic data were tested with parametric tests (independent samples T Test for 2 groups or one-way ANOVA for 3 or more groups). Non-normal distributed and/or heterocedastic data were tested with non-parametric tests (Mann-Whitney U Test for two groups or Kruskal-Wallis one-way analysis of variance for 3 or more groups). The statistical significance level chosen for all statistical tests was $p<0.05$.

7. Results

7.1. Implementation of the Neonatal Apex-Resection Model

In order to study the molecular mechanisms underlying cardiac regeneration we established the neonatal apex-resection model developed by Porrelo *et al.* (25), at our laboratory (Figure 6). Differently, we used the inbred C57Bl/6 strain instead of the outbred ICR/CD-1 strain originally used and post-natal (P2) mice instead of P1, since were still within the reported regenerative period (25). Survival rates were approximately 70% ± 22% post-surgery and 38% ± 36% after maternal cannibalism. Sham-operated animals, subjected to the same surgical procedure but without apex resection, were used to exclude misleading effects of the surgery. The survival rate in this group was significantly higher (approximately 85% ± 15% post-surgery and 55% ± 27% after maternal cannibalism).

Hearts of non-manipulated animals, sham-operated and apex-resected animals were harvested at different time-point to validate and characterize the injury model.

Histological characterization (Figure 7) demonstrated the reproducibility of the surgery as the majority of the lesions reached the cardiac lumen. In the first 48 hours post-resection (dpr), a large blood clot is formed (yellow and red staining in Masson's Trichrome and Hematoxilin-Eosin stain, respectively) to prevent extensive haemorrhage, as containment response, following exposition of the lumen after resection. As soon as 48 hours and up to 7 dpr an inflammatory-like infiltrate is observed at the injury site, which is replaced by a collagen rich-extracellular matrix (blue staining in Masson's Trichrome staining) from 14 dpr onwards. This scar region is still noticeable at 60 dpr which was the last time-point analysed. Of note, the observed collagen-based scar does not seem to extend to the whole apex but rather to the most central sections in which the apex is observed. Additionally, collagen rich adhesions become apparent in the epicardial surface of the cardiac apex at 5 dpr and were still present at 60 dpr. These adhesions, that tightly attached the heart to the ribs (data not shown), and are a common consequence of open-heart surgery, result from the inflammatory reaction created on outer surface of the heart. Overall, we observe an accumulation of fibrotic tissue in the myocardium and externally to the epicardium, which differs reported observations of a regenerative response with minimal cardiac fibrosis (25).

Functional characterization of the neonatal injury model was performed at 21 dpr and compared to sham-operated animals of the same time-point (Figure 8). The measures performed using M-mode images of the short-axis (SAX) and parasternal long-axis (PSLAX) allowed the determination of ejection fraction and fraction shortening. These indicators of systolic function and the left ventricle internal diameter during systole (LVIDs) were not statistically different between groups. However, left ventricle internal diameter during diastole (LVIDd) was increased in animals subjected to apex-resection (p-value < 0,05). These results demonstrate that tissue remodelling observed in the histological characterization, namely the apical collagen deposition, does not significantly impact on LV function. However, the differences in the LVIDd correlate well with a more round-shape anatomy observed in the apex-resected group (Supplementary Figure 1).

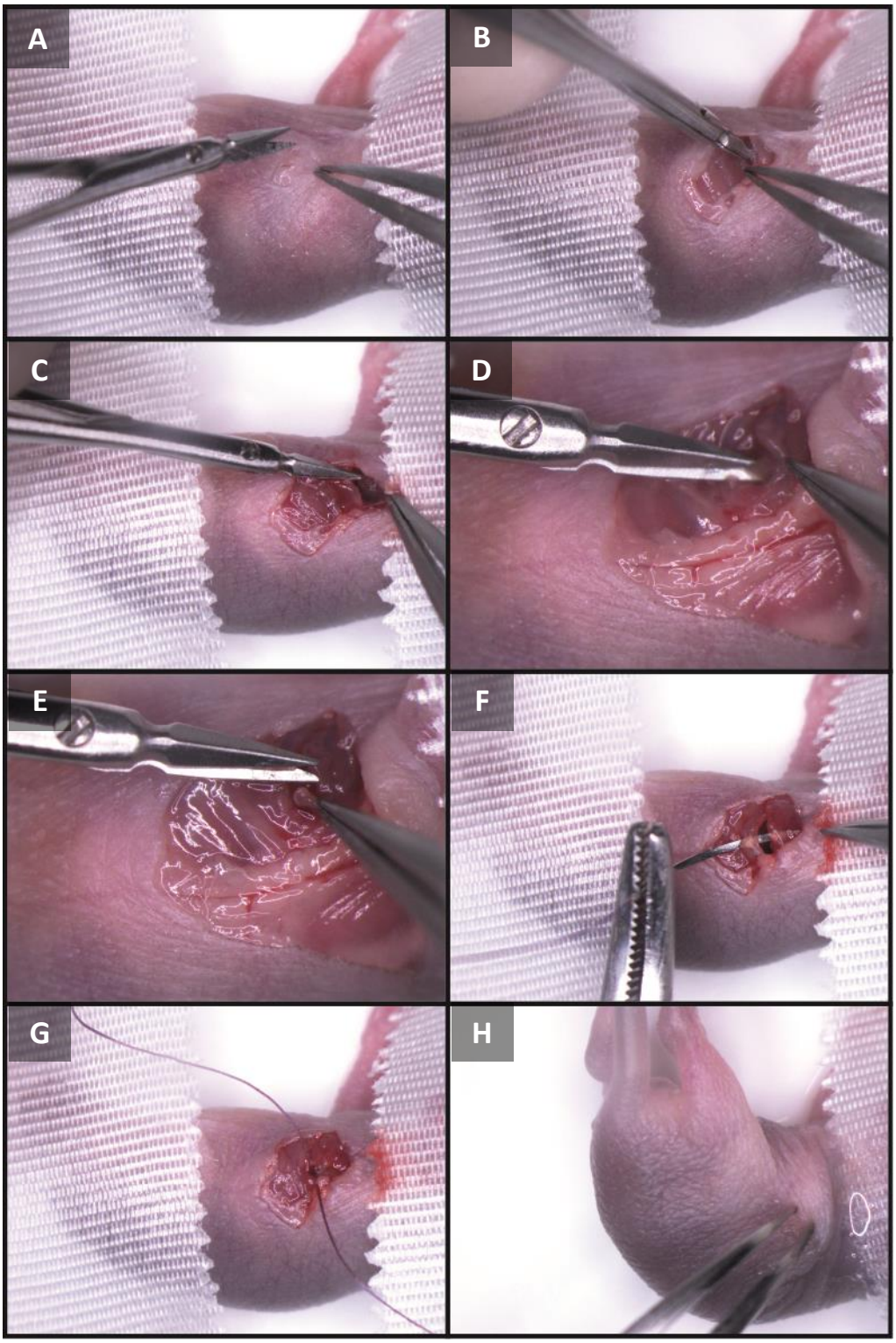

***Figure 6 – Neonatal Cardiac Injury Model**. After being anesthetized by hypothermia during 3 minutes, P2 C57BL/6 mice are laid in lateral decubitus position. The skin is cut and muscle fibers disrupted until the ribs are visible (A-B). The heart is assessed by opening the thorax in the 3rd intervertebral space and the apex is cut (C-E). The suture comprises two surgeon's knots that ligate the two separated ribs (F-G). The skin is glued using tissue adhesive (H) and respiratory and cardiac movements are recovered by subjecting the animal to heat produced by an infrared lamp.*

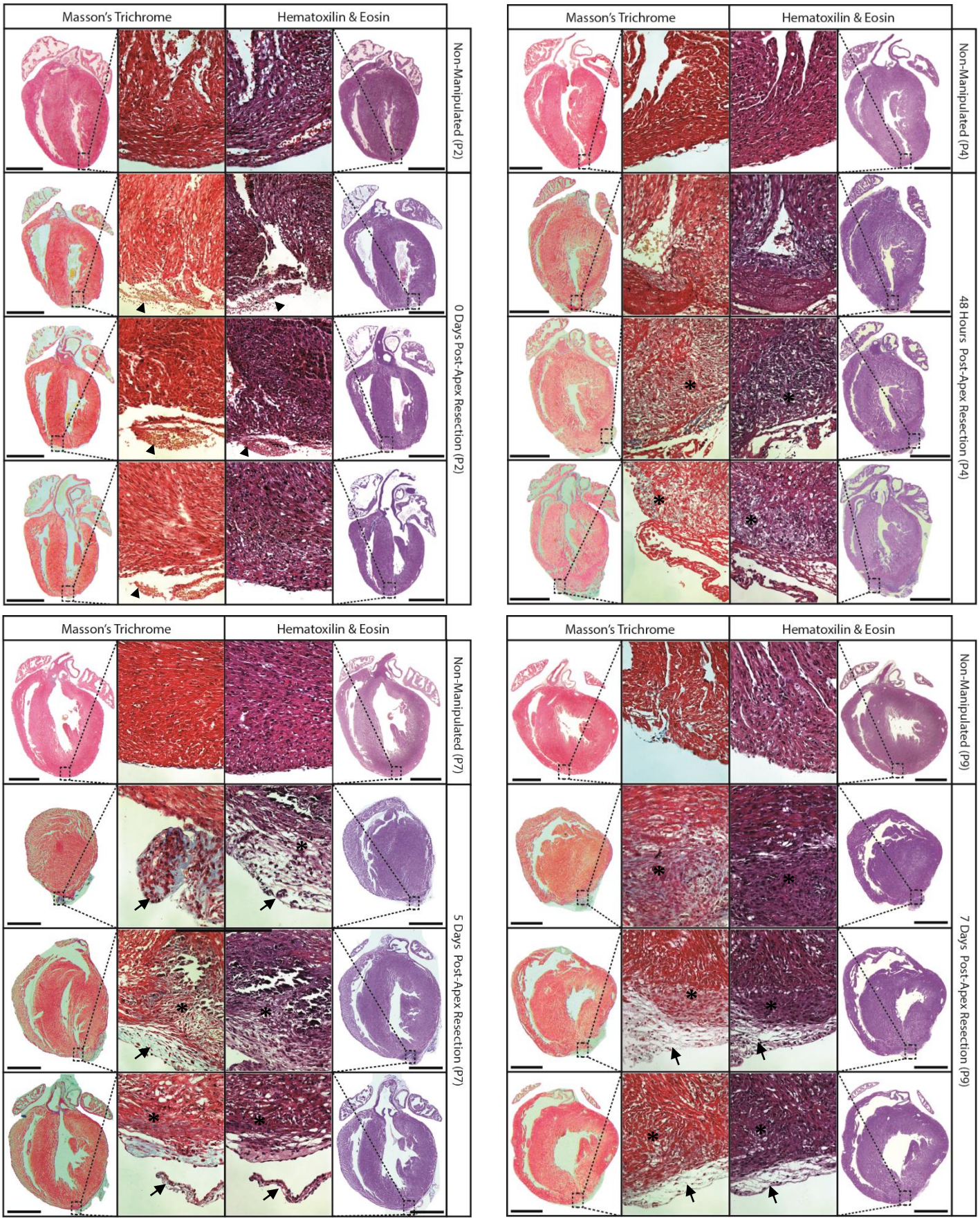
Masson's Trichrome
Hematoxilin & Eosin
Non-Manipulated (P2)
0 Days Post-Apex Resection (P2)
Masson's Trichrome
Hematoxilin & Eosin
Non-Manipulated (P4)
48 Hours Post-Apex Resection (P4)
Masson's Trichrome
Hematoxilin & Eosin
Non-Manipulated (P7)
5 Days Post-Apex Resection (P7)
Masson's Trichrome
Hematoxilin & Eosin
Non-Manipulated (P9)
7 Days Post-Apex Resection (P9)

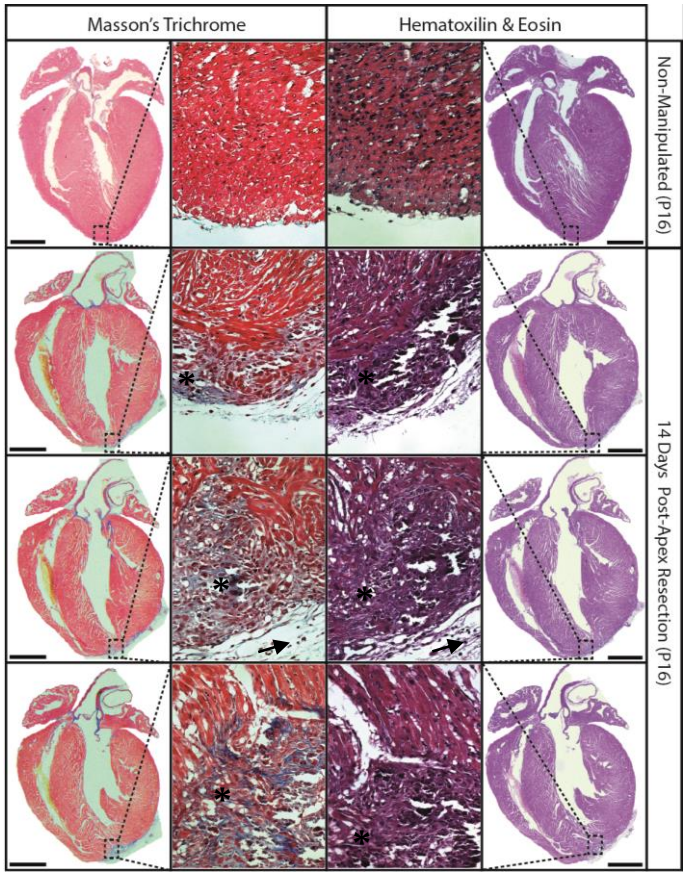

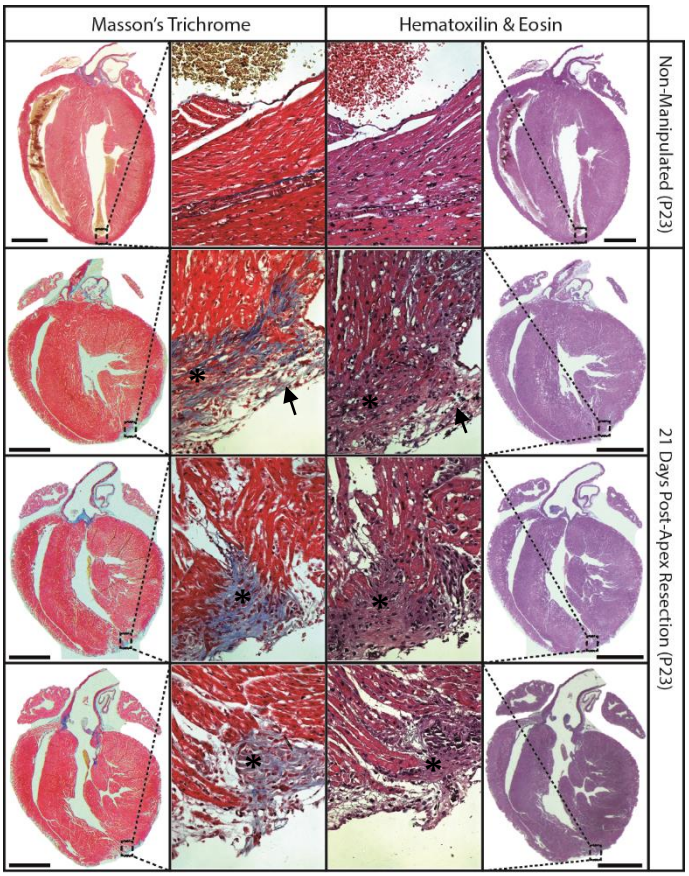

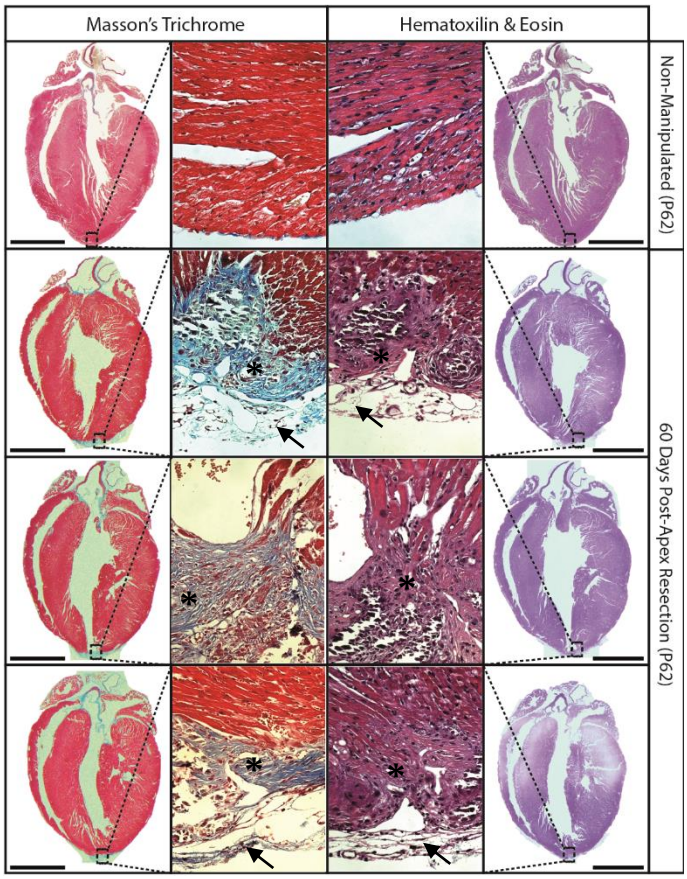

Figure 7 – Histological Characterization of the Neonatal Cardiac Injury Model. *Representative Masson's Trichrome (MT) and Hematoxilin-Eosin (HE)-stained sections of apex-resected hearts at specific timepoints (0, 2, 5, 7, 14, 21 and 60 days post-apex resection (dpr)) Their specific non-manipulated controls (P2, P4, P7, P9, P16, P23 and P62) are also shown. Only central sections, in which the apex region was more evident, were selected to the panel. Low power images emphasize the morphological progression of the heart following injury. High power images, focusing apex-resected area, show that as soon as 0 dpr until 48 hours post-surgery, a blood clot is formed (arrowheads). From 48 hours and up to 60 dpr, extensive tissue remodelling is evident at the apex region, culminating in the formation of a collagen-rich fibrotic scar (blue) that occupies part of the apex region (asterisk). Tissue adhesions are also visible in the epicardial surface of the heart in injured region. (arrows) Scale-bars: 1 mm (0, 2, 5, 7, 14, 21 dpr), 2 mm (60 dpr).*

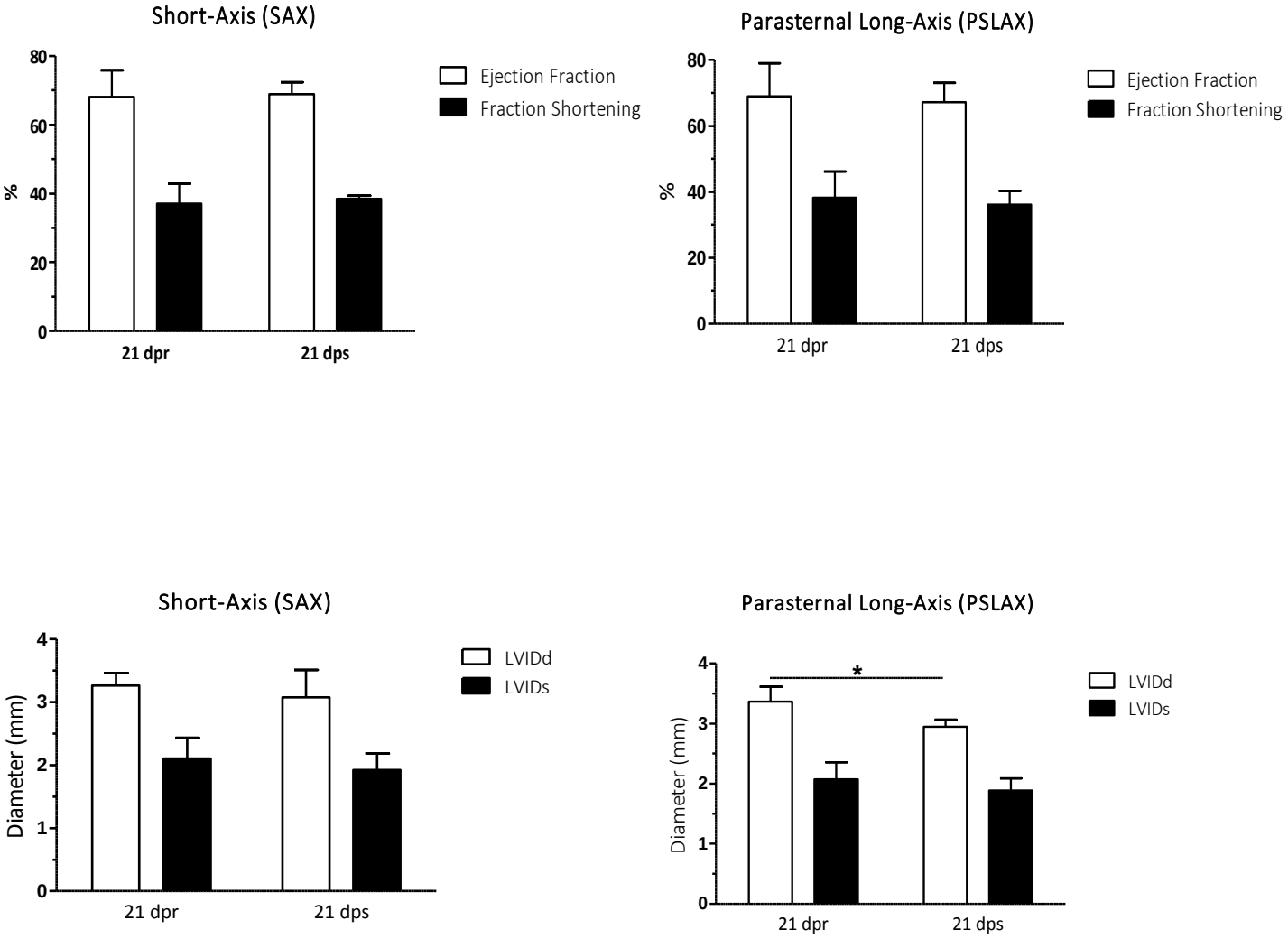

Figure 8 – Functional Characterization of the Neonatal Cardiac Injury Model. *Analysis of ejection fraction, fraction shortening, left ventricle internal diameter in diastole (LVIDd) and sistole (LVIDs), calculated in short-axis (SAX) and parasternal long-axis (PSLAX) view, of apex-resected mice (21 dpr, n=4) and sham-operated controls (21 dps, n=3). Apart from the LVIDd (p-value < 0,05), no differences were detected between apex-resected and sham-operated animals. Values are presented as means ± standard deviation (SD).*

7.2. Dynamics of the Cellular and Extracellular Compartments Following Apex-Resection

Several studies, namely in lower-vertebrates, have been focusing the role of ECM in heart regeneration. Here we ascribed the expression pattern of selected ECM proteins, namely fibronectin, tenascin-C, laminin and collagen IV. Additionally, we co-localized these proteins with different cardiac-cell markers, aiming at inferring which cell type is responsible for the production and secretion of such proteins (Figure 9). Therefore, we analysed the expression of sarcomeric-alpha-actinin (cardiomyocytes), CD45 (hematopoietic cells), alpha-smooth muscle actin (smooth muscle cells/myofibroblasts), CD31 (endothelial cells) and vimentin (fibroblasts).

Hematopoietic cells (CD45-expessing cells) are present from 0 dpr and cell frequency increases until 5dps while, from this time-point onwards, a dramatic decrease of CD45-expressing cells is observed which may relate with the resolution of inflammation. Differently, α-SMA- and vimentin-expressing cell rates steadily increase until 7 dpr, most likely representing the proliferation and differentiation of cardiac fibroblasts into myofibroblasts. Concordantly to what is described in literature for zebrafish and urodele amphibians, we observed increased deposition of fibronectin (FN) and tenascin-C (TN-C) in the outer surface of the apex-resected area. This accumulation is already evident at 48 hours post-apex resection and remains elevated until 14 dpr for fibronectin and until 21 dpr for tenascin-C. An association between fibronectin and CD45 expression was observed until 5 dpr. However, from 7dpr onwards, fibronectin appears augmented in the vicinity of alpha-smooth muscle actin (α-SMA) expressing cells. This is suggestive of a double origin of fibronectin at the injury site i.e. primarily the fibronectin originates from the blood clot and infiltrating inflammatory cells, while after resolution of acute inflammation, *de novo* fibronectin production is assured by myofibroblasts. Regarding TN-C expression, despite accumulated in regions in which vimentin expressing cells appear more frequently (in the border zone of the resected apex), vimentin expressing-cells do not seem to be the major producers of this protein. Through the expression of sarcomeric-alpha-actinin (s-α-actinin) we were able to observe myocardial disruption caused by apex-resection. However, as time progresses, there seems to occur a partial recovery of the myocardium. This is corroborated by the expression pattern of the basal lamina proteins laminin and collagen IV that normally form a sheath surrounding cardiomyocytes. At early time-points, there is a clear disturbance of the normal laminin and collagen IV expression patterns in the apex-resection area, which is almost recovered by 21 dpr. With regard to CD31 expression, we were only able to detect its presence on major vessels, and not on capillaries as was expected, in both injury- and sham-conditions which may relate to epitope masking due to fixation or the need for signal amplification.

Subsequently, we aimed to ascertain if the expression of extracellular matrix was correlated with higher levels of proliferation/mitosis. We focused at 5 and 7 dpr once higher levels of FN and TN-C were detected at these time-points. Also, in the original report of the neonatal apex model the proliferation was highest at 7 dpr. Once the combination of antibodies was not compatible with the co-detection of FN, TN-C and PH3, we first verified that the expression pattern of FN and TN-C overlapped (Figure 10) and then the expression α-actinin was co-localized with either PH3 or fibronectin in adjacent sections. As we hypothesized, the frequency of mitotic cells is higher in the injury site and within tissue adhesions, and thereby, in regions of/adjacent to FN and TN-C accumulation. These findings are suggestive that FN and/or TN-C might be promoting cell proliferation in the neonatal injured heart.

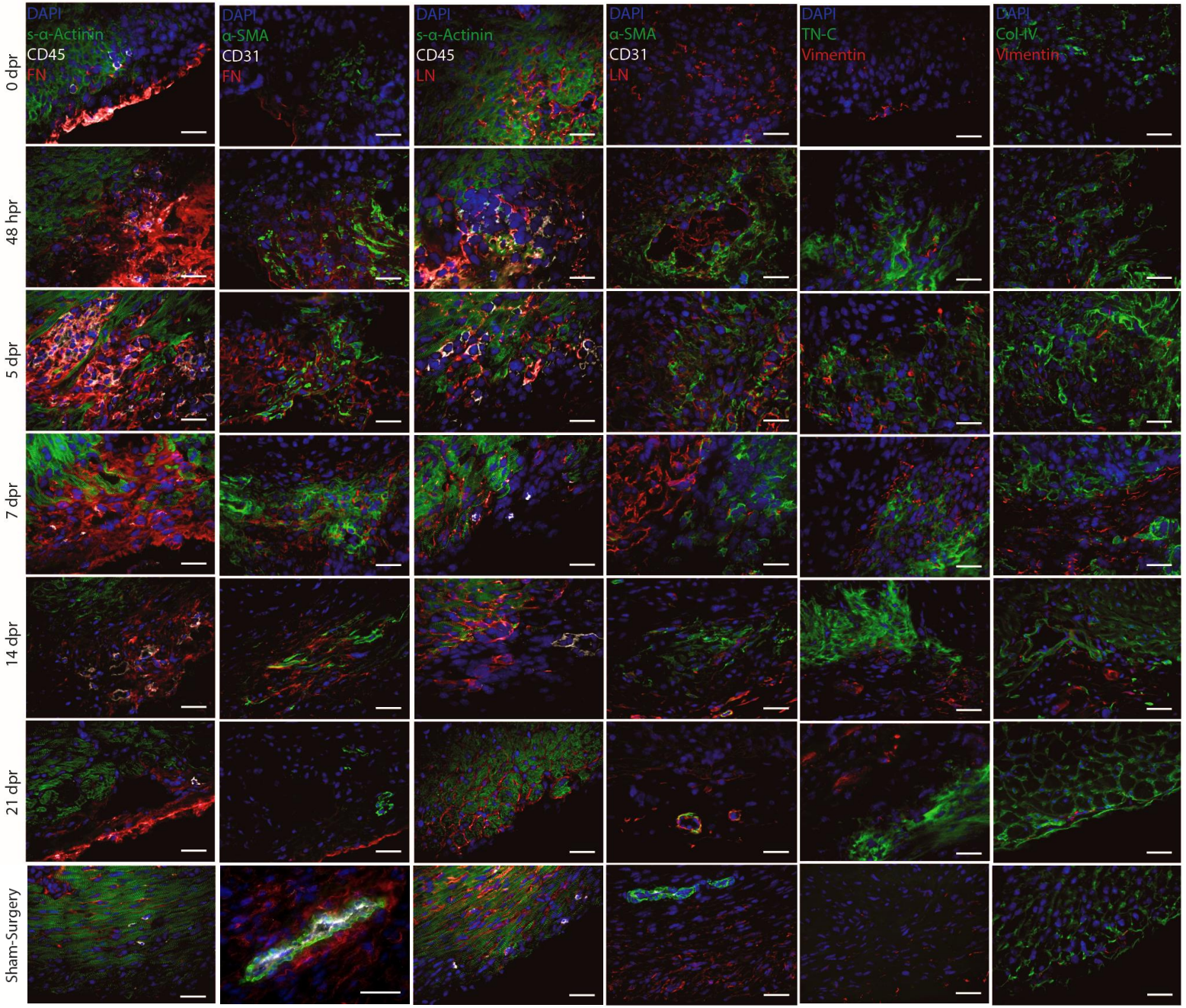

Figure 9 – Representative images of cardiac cells co-localization with ECM components in the injury site at 0, 2, 5, 7, 14 and 21 days post-apex resection. *The disruption of the myocardium caused by the apex-resection is shown by αActinin staining and by the disorganized pattern of the basal lamina proteins laminin and collagen IV until 14 days post-apex resection. From 48 hours up to 21 days following apex resection the cellular and extracellular composition of the injured site is dramatically altered, culminating in the partial reestablishment of the removed myocardium at 21dpr. Scale-bars, 30 µm; n=3.*

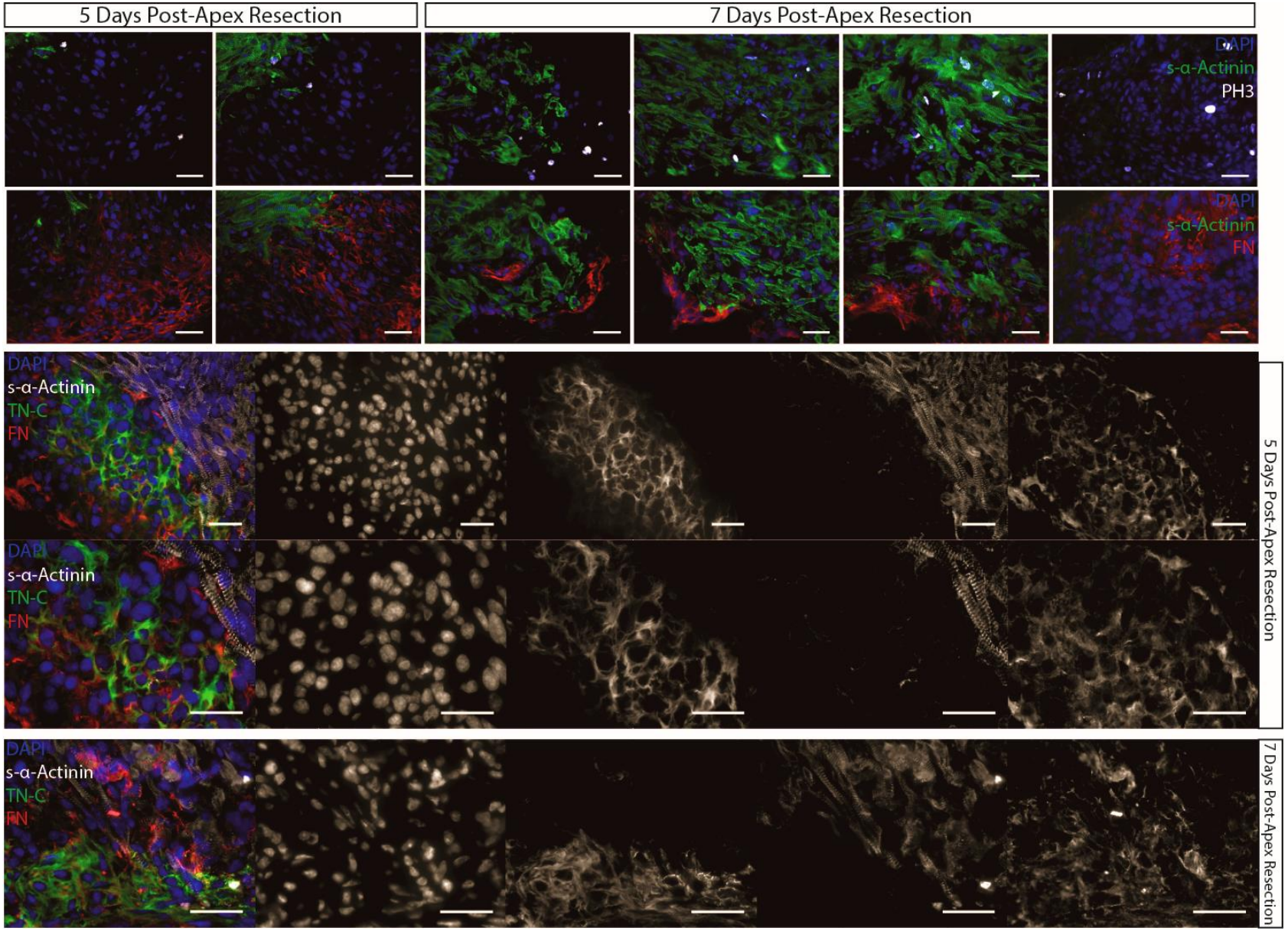

Figure 10* – Representative images of mitotic cells (*PH3⁺*) *in the vicinity of extracellular matrix deposition (fibronectin and tenascin) at 5 and 7 days post-apex resection. *Scale bar, 30 µm. n=2.*

With the purpose of determining the levels of proliferation, in particular of cardiomyocytes, in injured *vs* sham-operated hearts 7 days after surgery, co-localization of DAPI, s-α-Actinin and PH3 was performed and, whole-heart images were obtained via the assembly of high-magnification images. With appropriate software, we determined the number of mitotic cells (co-localization of DAPI and PH3) and the number of mitotic cardiomyocytes (co-localization of DAPI, PH3 and s-α-Actinin). The results revealed that the number of mitotic cells per mm^2, in the ventricles, is increased near the injury site, and therefore the analysis was restricted to the myocardial region bellow the papillary muscles (Supplementary Figure 3 and 4). This analysis showed that the proliferation (Figure 11A) and in particular of cardiomyocytes (Figure 11B), was increased in the apex-resected group when compared to the control, although this tendency did not reach statistical significance (p-value = 0,154 and p-value = 0,177, respectively). We consider that the statistical significance may be attained by increasing the numbers of analysed samples. This will also permit the identification of outliers in the sham operated group that may be generated as a result of unintentional scrapping of the myocardium during the disruption of the pericardium and that can activate injury mechanisms of cardiomyocytes proliferation as following apex-resection.

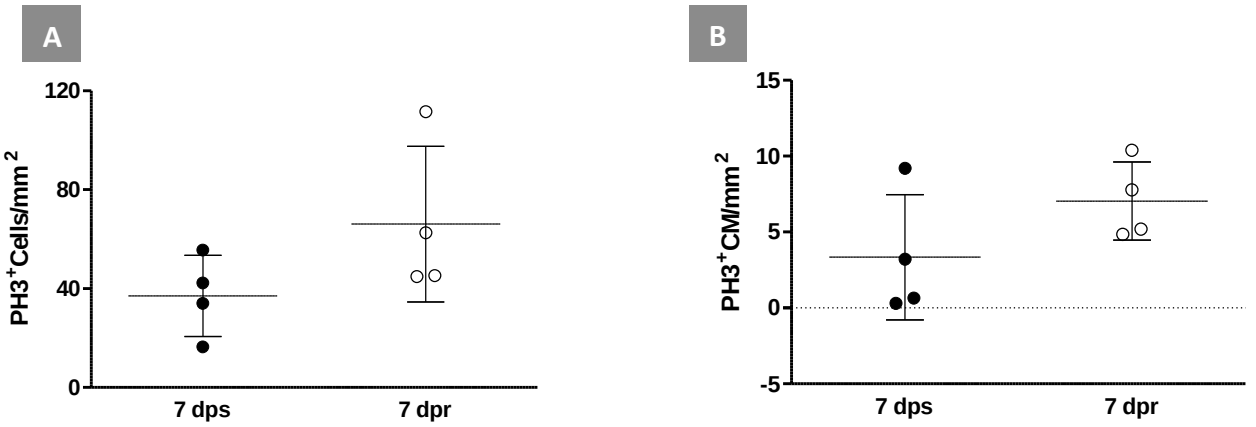

***Figure 11* – Proliferation on the ventricles (bellow papillary muscles) of apex-resected animals and sham-operated controls, 7 days post-surgery. *A* –** *Number of mitotic cells per mm^2 in the apex area. Despite the increased number of mitotic cells in the 7 dpr, no significant differences were found between groups (p-value = 0,154).* ***B* -** *Number of mitotic cardiomyocytes (CM) per mm^2. Despite the increased number of mitotic CM in the 7 dpr, no significant differences were found between groups (p-value = 0,177). n=4.*

7.3. Dynamics of Cardiac Fibroblast Populations Throughout Ontogeny and Following Apex-Resection

With the aim at characterizing the cardiac fibroblast populations throughout ontogeny, we digested the heart to obtain a single-cell suspension that was subjected to immunolabeling, with an assortment of antibody to discriminate different cardiac populations, and further analysed by flow-cytometry. To exclude endothelial, hematopoietic and erythroid cells, antibodies against CD31, CD45 and TER119, respectively, were included in the analysis. Propidium iodide (PI) assisted on the exclusion of death cells, once live cells do not incorporate this compound. The triple negative population ($CD31^-$, $CD45^-$ $TER119^-$) is the population selected for further analysis and is hereafter further called “the stroma” (Figure 12A).

Within this population, cardiac fibroblasts were identified on the basis of CD90 (Thy-1) expression (Figure 12A and B). At the embryonic day (E)17 the amount of CD90 expressing cells in the heart is around 30%, this frequency highly increases following birth reaching above 50% at P2. The numbers of cardiac fibroblasts ($CD90^+$) stabilizes at approximately 60% from P14 onwards. Despite the existence of a large variation on the levels of CD90 between embryonic (E17) and post-natal life (P2), this difference did not reach statistical significance. Significant differences were found between E17 and P10 (p-value < 0,05), E17 and P14 (p-value < 0,001); E17 and Adult (p-value < 0,01); P2 and P14 (p-value < 0,001), P2-Adult (p-value < 0,05); therefore supporting the observed tendency for $CD90^+$ increase throughout life.

As previously mentioned, we analysed the expression of mesenchymal-associated markers and cell-adhesion molecules together with $CD90^+$ population, namely CD29 (Integrinβ1), Sca-1 (Stem Cell Antigen 1), CD44, CD140a (PDGFRα), CD105 (Endoglin), CD106 (VCAM-1) (Figure 12C). Regarding the co-expression of CD90 and CD29, the large majority of CD90 expressing cells express CD29 in all analysed ontogenic stages. Still, statistically significant differences were found between E17 and P10 (p-value < 0,05), E17 and P14 (p-value < 0,05), P2 and P10 (p-value < 0,01), P2 and P14 (p-value < 0,001). The elevated frequency of $CD29^+CD90^+$ (>90%) casts doubt on the biological relevance of such small, though statistically significant, variations.

Recently, our team (10, 64) and others (65, 66) showed that mesenchymal-affiliated markers are commonly expressed by heart-resident $Sca\text{-}1^+$ progenitors and cardiac fibroblasts, reinforcing the impact of understanding the composition alongside the cardiogenic potential of the stromal cell compartment in the heart. We have analysed the frequency of $Sca\text{-}1^+$ cells within the $CD90^+$ population. $Sca\text{-}1^+CD90^+$ cells increase substantially throughout ontogeny, being almost negligible at E17/P2 while increasing to 30% and 70% at P14 and during adulthood, respectively. Indeed, statistically significant differences were found between E17 and P14 (p-value < 0,01), E17 and adult (p-value < 0,01), P2 and P14 (p-value < 0,001), P2 and adult (p-value < 0,001).

CD44 is a transmembrane glycoprotein that functions as cell-adhesion molecule, by tethering cells to extracellular ligands such as hyaluronic acid, but also participates in cell-signalling cascades (67). Additionally the expression of CD44 has been related to the differentiation of fibroblasts into myofibroblasts (68) and to fibroblast tissue-invasive capacity (69, 70). The percentage of $CD44^+CD90^+$ remained stable around 25% throughout ontogeny.

During development, PDGFRα (CD140a) is required for epicardial-specification and epicardial derived cells epithelial-to-mesenchymal transition that gives rise to a population of cardiac fibroblasts. Indeed, loss of PDGFRα, results in a specific disruption of cardiac fibroblast development and subsequent absence $PDGFR\alpha^+$ fibroblasts cells in the myocardium (71). Our results, demonstrate that the levels of $CD90^+CD140a^+$ fibroblasts increases from 60% in E17 up to almost 90% in P14, while re-establishing throughout adulthood the expression levels observed at E17. Statistically significant differences were found between E17 and P10 (p-value < 0,01), E17 and P14 (p-value < 0,001), P2 and P14 (p-value < 0,001), P14 and adult (p-value < 0,01).

Two other mesenchymal-associated markers have been included in this analysis, CD105 (endoglin) and CD106. The percentage $CD105^+CD90^+$ cells increases throughout ontogeny, being approximately 60% of at E17 and ranging between 80% from P2 to adulthood. Statistically significant differences were found between E17 and P14 (p-value < 0,05), E17 and adult (p-value < 0,05). Similarly, $CD106^+CD90^+$ became more frequent throughout ontogeny, starting at approximately 50% at E17 and stabilizing at 60-65% from P2 onwards. Significant differences were found between E17 and P2, P14, adult (p-value < 0,001), E17 and

P10 (p-value < 0,01). CD140b- (PDGFRβ) and Flk-1-expressing cells were also evaluated but negligible percentages were found within the CD90 cell-compartment (Supplementary Figure 2).

We further analysed the proliferative behaviour of the stromal compartment ($CD31^-CD45^-TER119^-$) throughout ontogeny, using the proliferation marker Ki67 (Figure 12D). Concordantly to what is described in literature, the number of proliferating cardiac cells declines considerably throughout ontogeny. At E17 over 30% of the cells are proliferating while, this percentage progressively decreases reaching a minimum of 2-3% in the adult life. Statistically significant differences were found between E17 and P14 (p-value < 0,01), E17 and adult (p-value < 0,001), P2 and P14 (p-value < 0,05), P2 and adult (p-value < 0,01).

Within the proliferative compartment ($CD31^-CD45^-TER119^-Ki67^+$), we evaluated the expression levels of CD90, Sca-1, CD44 and CD29 (Figure 12E). Regarding the co-expression of Ki67 and CD90, a slight increase throughout ontogeny is observed. At E17 the percentage of proliferating $CD90^+$ cells is approximately 40%, reaching 60% at P14. Statistically significant differences were found between E17 and P10 (p-value < 0,01), E17 and P14 (p-value < 0,05), P2 and P10 (p-value < 0,05). The expression of Sca-1 within the proliferative compartment also increases throughout ontogeny, starting at approximately 5% at E17 and reaching the maximum of approximately 80% in the adult. Statistically significant differences were found between E17 and P14 (p-value < 0,05), E17 and adult (p-value < 0,01), P2 and adult (p-value < 0,01). These results are consistent with the augmentation of $CD90^+$ and is particular, $CD90^+Sca\text{-}1^+$ throughout ontogeny. The proliferative compartment is mainly composed of cells with CD29 (integrin-β1) at their surface throughout ontogeny. However, a small, but statistical significant, reduction on the expression levels of this marker was observed post-birth. Once again, the biological relevance of such minor reduction is at present challenging to envisage. The percentage of $CD44^+$ within the proliferative compartment increased throughout ontogeny. Statistically significant differences were found between P10 and P14 (p-value < 0,001), P10 and adult (p-value < 0,01).

We used the same approach to characterize the cardiac fibroblast population in apex-resected and sham operated animals at 7 days post-surgery (Figure 13A). Although the percentage of $CD90^+$ cells was identical between groups, a significant decrease was observed in the frequency of $CD140a^+$ (p-value < 0,01) and $CD29^+$ (p-value < 0,05) cells together with an increase in the $CD44^+CD90^+$ and $Sca\text{-}1^+CD90^+$ cell compartments (p-value < 0,01 and 0,05, respectively). Once more, the percentage of CD140b- and Flk-1-expressing cells in the $CD90^+$ compartment was negligible (Data not shown). Considering the proliferation in the stromal compartment (Figure 13B) no statistically significant differences were found on Ki67 expression levels between injury and sham-operated animals. However, the percentage of $Sca\text{-}1^+$ cells (p-value < 0,001) within the proliferative compartment has almost doubled in injury conditions, when compared to sham-operated animals.

A

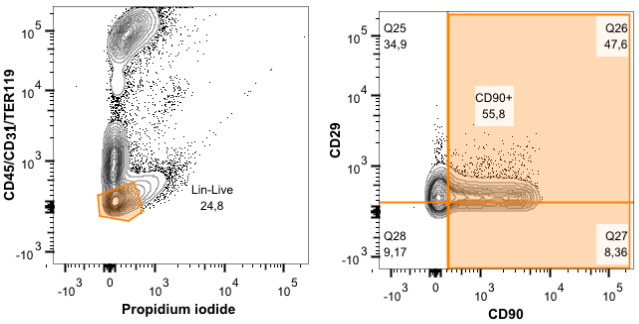
CD45/CD31/TER119
Propidium iodide
Lin-Live
24,8
CD29
CD90
Q25
34,9
Q26
47,6
CD90+
55,8
Q28
9,17
Q27
8,36

B

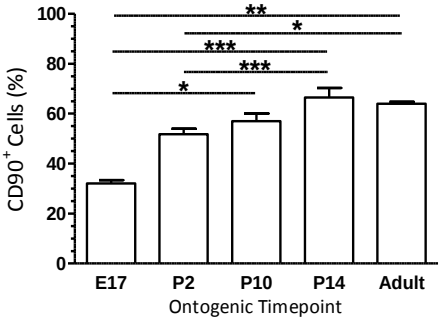
CD90+ Cells (%)
E17
P2
P10
P14
Adult
Ontogenic Timepoint

C

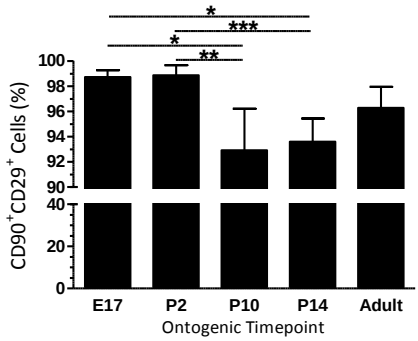
CD90+CD29+ Cells (%)
E17
P2
P10
P14
Adult
Ontogenic Timepoint

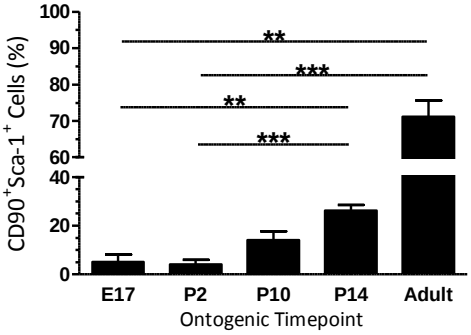
CD90+Sca-1+ Cells (%)
E17
P2
P10
P14
Adult
Ontogenic Timepoint

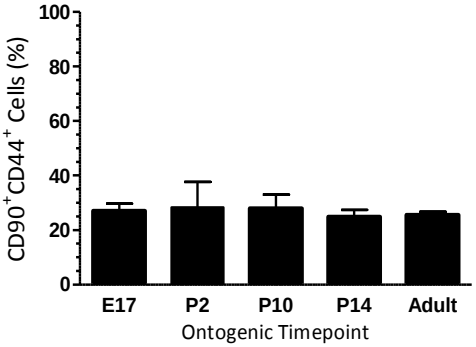
CD90+CD44+ Cells (%)
E17
P2
P10
P14
Adult
Ontogenic Timepoint

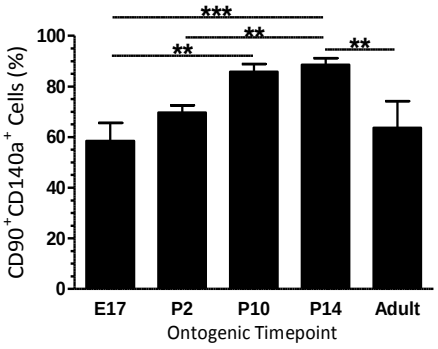
CD90+CD140a+ Cells (%)
E17
P2
P10
P14
Adult
Ontogenic Timepoint

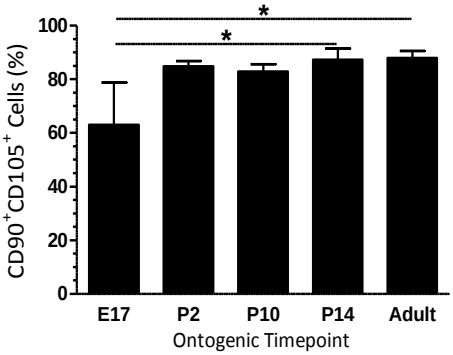
CD90+CD105+ Cells (%)
E17
P2
P10
P14
Adult
Ontogenic Timepoint

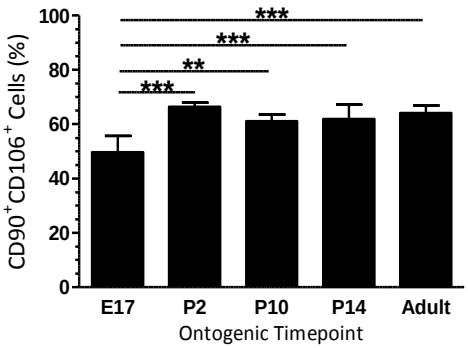
CD90+CD106+ Cells (%)
E17
P2
P10
P14
Adult
Ontogenic Timepoint

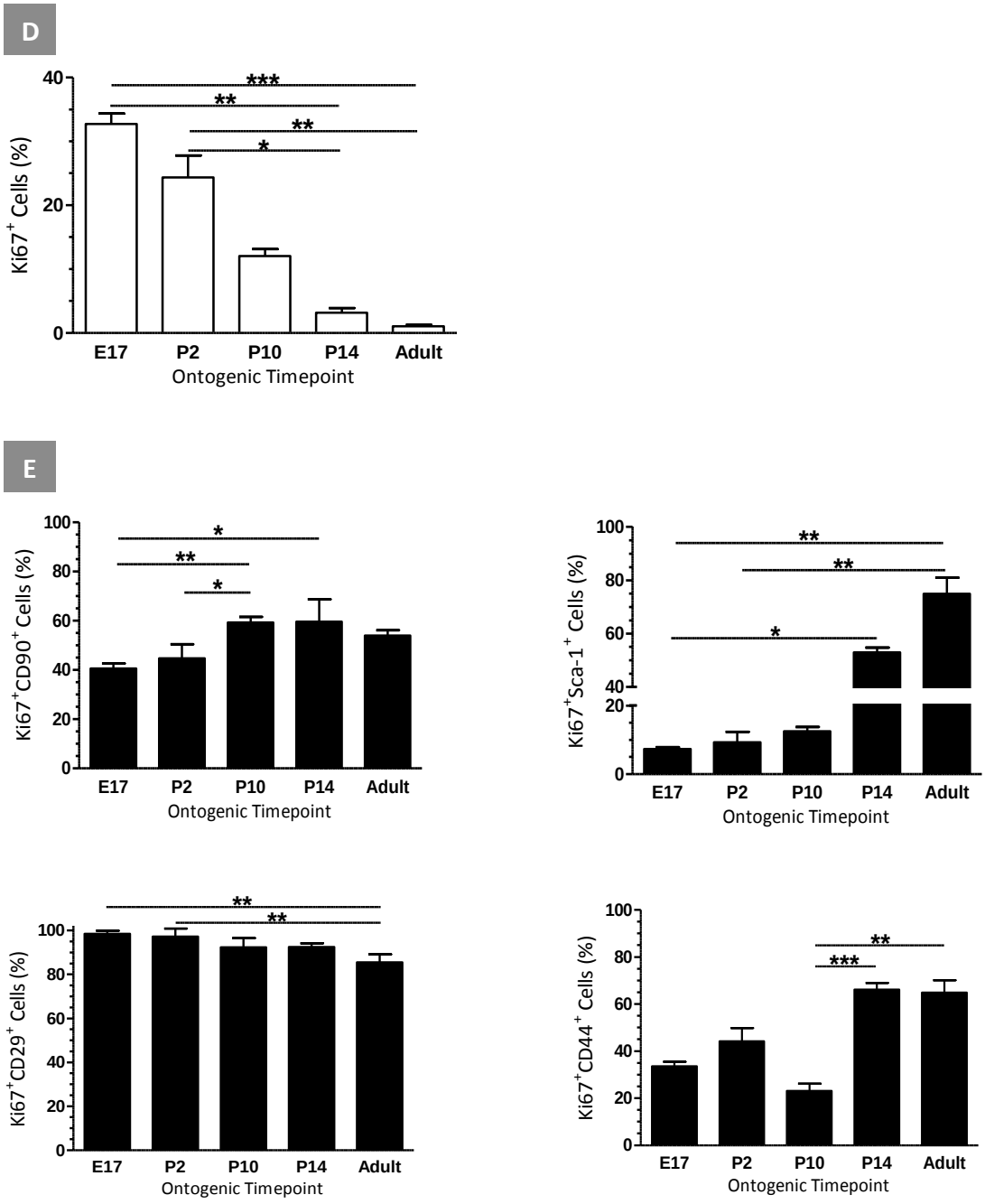

Figure 12 – A *– Pheontypic characterization of cardiac fibroblasts (CD90⁺CD45 CD31⁻TER119⁻) throughout ontogeny. Hematopoietic (CD45⁺), endothelial (CD31⁺) and erythroid cells (TER119⁺) were excluded from the analysis. Within the stromal compartment i.e. CD45⁻CD31⁻TER119⁻, cardiac fibroblasts were identified by the expression of CD90 (**B**). The expression of mesenchymal-affiliated marker and adhesion molucules was further investigated in the CD90+ fibroblasts (**C**). E17 (n=6); P2 (n=11); P10 (n=11); P14 (n=11); Adult (n=4). The stromal proliferative compartment, trougout ontogeny, was ascribed by Ki67 expression profile (**D**) and finne characterized (**E**). E17 (n=4); P2 (n=7); P10 (n=8); P14 (n=8); Adult (n=4). * (p-value < 0,05), ** (p-value < 0,01), *** (p-value < 0,001).*

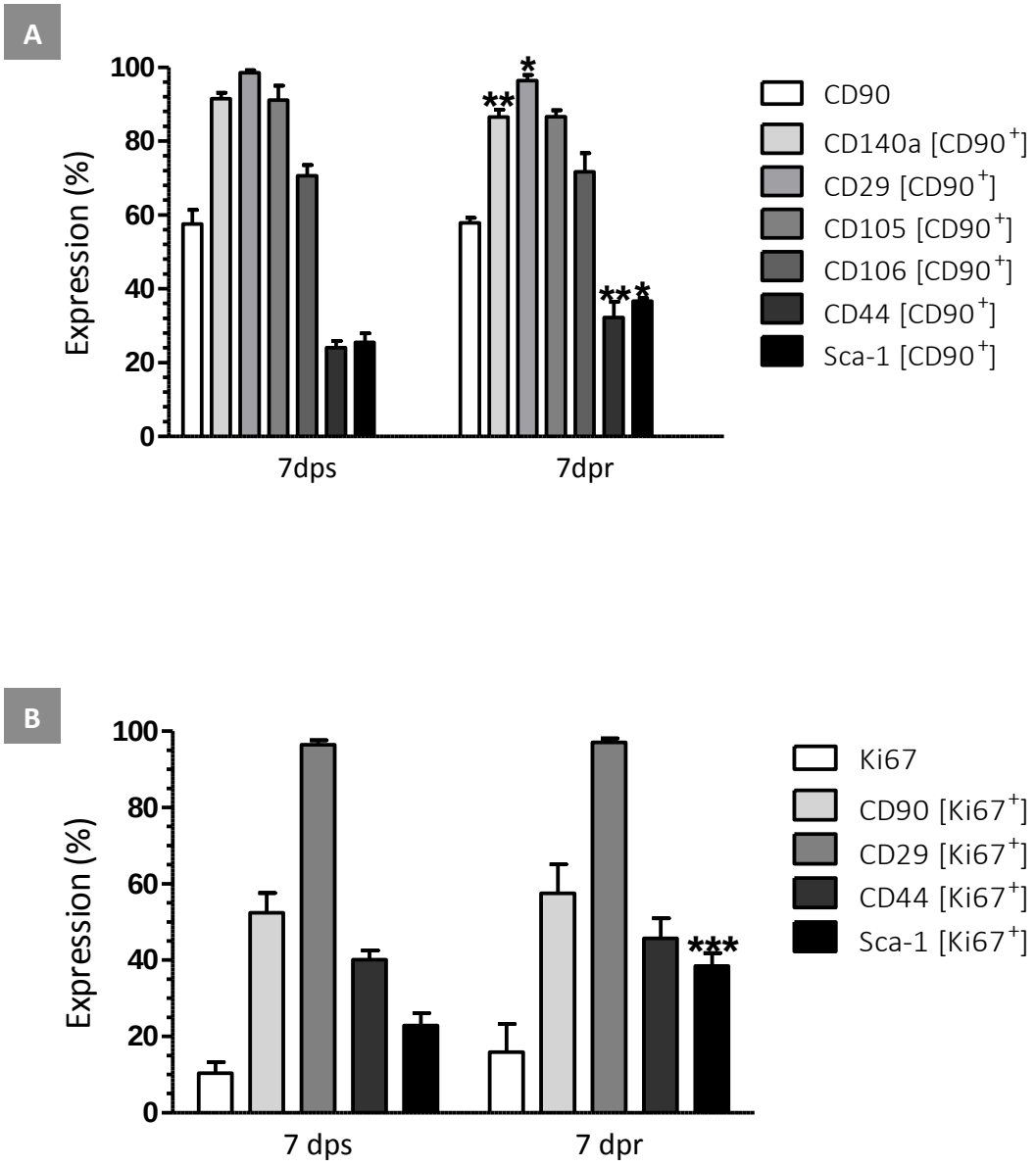

Figure 13 – A *- Dynamics of Cardiac Fibroblast Populations 7 days after apex-resection. CD90 expression profile of the stromal compartment (CD31-CD45-TER119-) population was investigated post-apex resection (dpr) and post-sham surgery (dps) [white bars].* ***B –*** Dissection of proliferative populations of the heart stroma (CD31-CD45-TER119-) activated 7 dpr. ** (p-value < 0,05), ** (p-value < 0,01), *** (p-value < 0,001).* (n=5, 7 dpr); (n=6, 7 dps).

8. Discussion

In 2008, cardiovascular diseases were responsible for approximately 17,3 million deaths, representing 30% of global mortality. Presently, heart conditions are ranked first in mortality causes worldwide and the available projections point for the prevalence of this tendency (72, 73). As the only long term effective therapy for heart failure rely on cardiac transplantation, the scientific community has focused on the identification of cues that can promote cardiac regeneration or, to the least, lead to improved repair following injury.
Heart regeneration was first observed in lower vertebrates such as zebra-fish and urodele amphibians. Despite the long phylogenetic distance between these organisms and mammals, in 2011 Porrello *et al*. reported that murine hearts fully recovered from apex-resection within 21 days, as long as it was performed during the first week of life. In contrast, after inflicting the same lesion in 7 days old mice, the heart appeared to engage on a reparative response that encompasses the formation of a collagen-rich scar, thus resulting in the deterioration of cardiac function (25). This ground-breaking work demonstrated the intrinsic regenerative potential of the mammalian heart, which holds great promise for the development of novel therapeutic approaches. In the following years others have replicated the neonatal regenerative response using different models of cardiac injury (26–29). However in 2014, Andersen *et al.* refuted the existence of cardiac regeneration in mice, by reporting a scar-based response in neonatal apex-resected mice, questioning the usefulness of this model to study the molecular mechanisms underlying regeneration of the adult heart after damage.

The herein work aims to determine the dynamics of the cardiac fibroblasts and of ECM in neonatal cardiac injury. Therefore, we established the neonatal apex-resection model at our laboratory (Figure 6). The mice strain and the neonatal day in our model are different from the original report, which may account for differential results/outcomes. Nevertheless, the surgery is performed in P2 neonates, which are still within the reported neonatal regenerative window.

Regarding the histological characterization, the results show that, in our experimental setting, apex-resected hearts do not completely regenerate 2 months after surgery since collagen-rich extracellular matrix depositions are noticeable and spreading from the resected apex to the ventricular lumen (Figure 7). In this particular aspect, our results support the recent claim that neonates do not undergo complete regeneration. However, the scarring herein reported is not extended to the total apex but rather restricted to central sections, which is suggestive of an incomplete reestablishment of the apex. In this scenario, regenerative mechanisms would have to be activated to induce partial tissue growth being however insufficient for full histological restoration. Moreover, apex-resected animals displayed preserved systolic function, here assessed by ejection fraction and fraction shortening at 21 days post-surgery, when compared to sham-operated animals (Figure 8). Indeed, the only altered parameter was the LVIDd in the long-axis, which might relate with small left-ventricle dilation that did not produce a detectable impact on cardiac function.

To further understand the cellular and extracellular compartments actively involved in the neonate response to injury, we co-localized markers of cardiomyocytes, smooth muscle cells/myofibroblasts, fibroblasts, hematopoietic and endothelial cells with several extracellular matrix proteins, namely: fibronectin, laminin, collagen IV and tenascin-C (Figure 9).
Unsurprisingly, as consequence of apex-resection, a disruption on the expression pattern of s-α-actinin, laminin and collagen IV was noticeable. However, at 21 dpr their expression patterns were partly restored, suggesting a partial recovery of the heart.

The neonatal apex response seems to encompass the formation of a fibronectin-rich blood clot, followed by the establishment of a strong inflammatory reaction that peaks around day 5, given the accumulation of CD45-expressing cells at the injury site. Nevertheless, a dramatic reduction in the abundance of CD45 is observed between 5 and 7 days post-surgery which appear to correlate with an increase in fibroblasts (vimentin) and myofibroblasts (α-SMA), abundant cell-types at this time-point. At 21 dpr, the inflammatory process seems to be resolved (the number of CD45 expressing cells returned to sham-operated levels) and myofibroblasts have been removed from the injured area. Interestingly, fibronectin and tenascin-C expression overlaps with areas of hematopoietic cells ($CD45^{+}$) and myofibroblasts ($\alpha\text{-SMA}^{+}$). These ECM proteins are significantly up-regulated from 48 hpr and remain overexpressed until 14 dpr (fibronectin) and 21 dpr (tenascin-C). Our results suggest that the augmentation of fibronectin has a triple origin depending on the time post-surgery. Hence, during the first 48h fibronectin originates in the blood clot, since is an abundant soluble constituent of blood plasma (74). During the inflammatory phase (48 hour to 5 days post-resection), fibronectin seems to be produced by hematopoietic cells. On the other hand, following inflammation dimming, myofibroblasts produce *de novo* fibronectin, given the co-localization of both expression patterns. Tenascin-C and α-SMA co-detection was not possible because of technical limitations; however, owing to the similarity in the deposition of both proteins in the injured area, we speculate that myofibroblasts may also contribute to tenascin-C production and secretion. Fibronectin and tenascin-C deposition is also observed following cardiac injury in zebrafish (60, 61) and newt (62). Fibronectin mediates a wide variety of cellular interactions and has been suggested to mediate the opsonisation of tissue debris, migration, proliferation and contraction of cells involved in tissue regeneration as well as in angiogenesis (75). In zebrafish, injury-mediated fibronectin deposition is fundamental to promote cardiomyocyte migration to the injury site while not affecting specifically their proliferation (60). In newt, fibronectin is part of a regenerative ECM, alongside tenascin-C and hyaluronic acid, which promotes cardiomyocytes cell-cycle reentry (62). Hyaluronic acid is known to provide a hydrated environment and tenascin-C, in turn, is known to have counter-adhesive domains (61, 62). Altogether, the accumulation of these molecules in the damaged myocardium likely improves cell migration to the injury site.

To investigate whether fibronectin and tenascin-C were promoting cell proliferation and/or migration of proliferative cardiomyocytes we verified that the deposition of these ECM components overlap at the injury site, followed by co-detection of fibronectin with proliferating cardiomyocytes ($\text{s-}\alpha\text{-actinin}^{+}\text{PH3}^{+}$) (Figure 10). Higher mitotic levels were observed in areas of fibronectin deposition as well as in the adjacent myocardium. Proliferation in the injury site is mainly observed in hematopoietic cells ($CD45^{+}$) and myofibroblasts ($\alpha\text{-SMA}^{+}$) (data not shown) whereas in the neighbouring myocardium proliferation is mostly observed in cardiomyocytes. Moreover, high-content imaging analysis showed that, at 7 days post-surgery, proliferation was augmented in that apex region, and in particular of cardiomyocytes, when compared to sham-operated control group.

Overall, our results demonstrate that the neonatal injury response at P2 involves the formation of a blood clot, recruitment of inflammatory cells, myofibroblasts proliferation and ECM remodelling that encompassed the production of fibronectin and tenascin-C. Although, these mechanisms are part of regenerative response observed in lower vertebrates, they are also a common feature of the reparative response observed in the adult mammalian heart (76–78) and therefore cannot argue in favour of the hypothesis of neonatal regeneration. Nonetheless, neomyogenesis is a particular feature of neonatal response to injury (25, 27, 79), and

differentiates neonatal heart compared to the adult mouse heart. Herein, evidence is provided for that, following apex-resection, P2 hearts activate mechanisms of cardiomyocyte proliferation which account for higher myocyte proliferation rates found in injured animals when compared to the sham-control. However, unlike initial claims of regeneration with negligible levels of fibrosis, our results demonstrate that fibrotic mechanisms are activated as such that a transmural scar is also formed in the central region of the apex. To wrap up, we find evidence for conserved regenerative mechanisms that seem to be activated following neonatal injury, although still at a level insufficient for full-reestablishment of the native tissue integrity.

Fibroblasts are activated following neonatal injury and seem to contribute by at least differentiating into myofibroblasts which are main ECM producers. Aiming at dissecting the fibroblast population/s involved in this processes, and because neonatal fibroblast populations have not been well characterized, we initiated a study to phenotypically portray fibroblast population/s, selected on the basis of CD90 expression ($CD31^{-}CD45^{-}TER119^{-}CD90^{+}$), throughout ontogeny. The number of CD90 expressing cells in the stromal compartment significantly increased all through development, which is concordant with the presently recognized idea that the majority of fibroblast colonize the myocardium after birth (33, 80, 81) (Figure 12B). Within the cardiac fibroblast population we established the expression profile of CD29, Sca-1, CD44, CD140a, CD105 and CD106 (Figure 12C). The large majority of cardiac fibroblasts (>90%), independently of the ontogenic stage, display CD29 (β1-integrin) at their surface. Sca-1 has been commonly used to identify CPCs, however this protein is generally expressed in mesoderm-derived cells and is not restricted to stem/progenitor cells. In fact, the cardiac $Sca\text{-}1^{+}$ CPCs has been shown to be highly heterogeneous, displaying features commonly associated with fibroblasts (10). Not surprisingly, we detected a significant increase throughout ontogeny of the $Sca\text{-}1^{+}$ $CD90^{+}$ population, suggesting that approximately 70% of adult cardiac fibroblasts express Sca-1. Similarly to Sca-1, CD140a, CD105 and CD106 are widely expressed in cells of mesenchymal origin, such as fibroblasts. Each of these markers was significantly increased throughout development, which accounts for the fact that fibroblasts are considered a heterogeneous population. CD44 is known to be a hyaluronic acid receptor, although it can interact with other ligands (82). Additionally, CD44-dependent activation of TGF-β signalling was associated with fibroblast activation and posterior migration to injury sites (83). As anticipated, we did not observe significant changes in the expression of CD44 by cardiac fibroblasts throughout ontogeny since no injury stimulus was provided.
Owing to a seemingly increase in fibroblasts throughout ontogeny we then hypothesized that these cells are the main contributors to the proliferation observed in the stromal population. To test this premise we analysed the dynamics of the stromal proliferative compartment ($CD31^{-}CD45^{-}TER119^{-}Ki67^{+}$), which as described in the literature, is severely reduced with aging (5, 6) (Figure 12D). Within the proliferative compartment a phenotypic switch between the fetal and adult life could be detected. While at E17, the majority of proliferative cells are $Sca\text{-}1^{-}$ and $CD90^{-}$, in the adult life the majority of the proliferative compartment expresses these markers. Interestingly, all proliferating cells are expressing CD29 regardless of the ontogenic stage. Overall these results indicate that the majority of proliferating cells in the adult heart stromal compartment are $CD90^{+}$ cardiac fibroblasts. Of importance, $Sca\text{-}1^{+}$ cells comprise more than 70% of the proliferating cells, whether these cells are fibroblast or so called CPCs is yet to be analysed.

To determine if specific populations of cardiac fibroblasts are activated upon neonatal heart injury we evaluated the expression levels of the aforementioned proteins in apex-resected and

sham-operated animals 7 days post-surgery. A statistical significant reduction on frequency of CD140a^{+} and CD29^{+} within the CD90^{+} population of cardiac fibroblasts was observed. Both switches involve minor changes, although, when considering that the injury only affects a small fraction of the heart, it is our perception that all differences should be considered and subjected to further analysis. Contrarily to CD140a^{+} and CD29^{+}, Sca-1^{+} and CD44^{+} cardiac fibroblasts are more abundant in apex-resected animals. Indeed both Sca-1^{+} and CD44^{+} are reported to be activated in injury situations in the adult heart. While Sca-1^{+} cells activated upon MI have been associated to a progenitor-like phenotype (65, 84, 85), up-regulation of CD44 relates with activation of fibroblasts (83). Nonetheless, when the proliferation is analysed following apex-resection, Sca-1^{+} cells are the only population that displays higher proliferative rates. Further studies are required to investigate the functional relevance of these populations either in normal heart physiology and following activation during neonatal injury response.

9. Conclusion

Here we demonstrate that the neonatal heart injury response at P2 involves the formation of a blood clot, recruitment of inflammatory cells, myofibroblasts proliferation, ECM remodelling (production of fibronectin and tenascin-C) and activation of cardiomyocytes proliferation. Also, alike Andersen *et al.* we were not able to observe a complete restoration of the apex following cardiac injury, instead, cardiac fibrosis was observed although confined to the most central portion of the resected area. In fact, the model that best suits our data suggests that following apex resection, a blood clot is formed to prevent extensive haemorrhage. Then, ECM remodelling occurs, with the deposition of fibronectin and tenascin-C, firstly associated to hematopoietic cells and later to fibroblasts/myofibroblasts. This scenario likely promotes cardiomyocyte proliferation and migration towards the injured area, partially recovering the lost apex. In the innermost region of the apex, where the lumen was exposed, cardiomyocyte turnover is not sufficient to ensure complete repopulation and cardiac fibrosis arise (Figure 14)

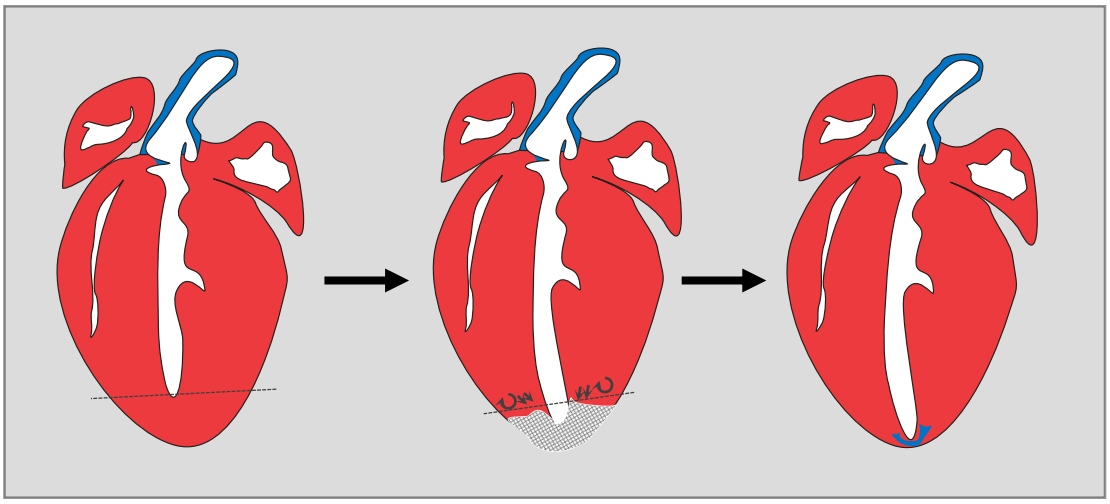

Figure 14 – *Model proposed for the biological mechanisms underlying neonatal cardiac injury. After resection, a blood clot is formed and is gradually replaced by proliferating fibroblasts and myofibroblasts. Concomitantly, ECM remodelling occurs by accumulation of fibronectin and tenascin-C, initially associated with hematopoietic cells and afterwards with fibroblasts/myofibroblasts. While this environment assists cardiomyocyte migration and proliferation from the neighbouring myocardium to the apex, at the central region, where the lumen was exposed, cell repopulation is insufficient and cardiac fibrosis settles.*

Still, further studies are needed to improve the statistical robustness of these results and to investigate the functional relevance of the observed ECM dynamics.

The ontogenic phenotyping of the heart stroma showed that $CD90^+$ fibroblasts colonize the heart following birth and that constitute the majority of proliferating cells throughout adulthood. $CD90^+$ cardiac fibroblasts suffer a phenotypic switch with aging, which is clearly exemplified by increase on the percentage of $Sca\text{-}1^+$ from residual levels at P2 to 70% in adult life. Interestingly, $CD90^+Sca\text{-}1^+$ cells seem to be activated following neonatal heart injury. The functional relevance of this observation is yet to be assessed.

10. References

1. Yusuf S et al. Effect of potentially modifiable risk factors associated with myocardial infarction in 5 countries (the INTERHEART study) case-control study. *Lancet*. 2004;:1–16.

2. Celermajer DS, Chow CK, Marijon E, Anstey NM, Woo KS. Cardiovascular disease in the developing world: prevalences, patterns, and the potential of early disease detection. [Internet]. *J Am Coll Cardiol*. 2012;60(14):1207–16.

3. Ott HC et al. Perfusion-decellularized matrix: using nature's platform to engineer a bioartificial heart. [Internet]. *Nat Med*. 2008;14(2):213–21.

4. John R et al. Long-term outcomes after cardiac transplantation: an experience based on different eras of immunosuppressive therapy. [Internet]. *Ann Thorac Surg*. 2001;72(2):440–9.

5. Beltrami AP et al. Evidence that Human Cardiac Myocytes Divide After Myocardial Infarction. *N Engl J Med*. 2001;344(23):1750–1757.

6. Bergmann O et al. Evidence for Cardiomyocyte Renewal in Humans. *Science (80-)*. 2009;324(98):98–102.

7. Hsieh PCH et al. Evidence from a genetic fate-mapping study that stem cells refresh adult mammalian cardiomyocytes after injury. *Nat Med*. 2007;13(8):970–974.

8. Ellison G et al. Adult c-kit+ Cardiac Stem Cells Are Necessary and Sufficient for Functional Cardiac Regeneration and Repair. *Cell*. 2013;154:827–842.

9. Torella D, Ellison GM, Karakikes I, Nadal-Ginard B. Resident cardiac stem cells. [Internet]. *Cell Mol Life Sci*. 2007;64:661–73.

10. Valente M, Nascimento DS, Cumano A, Pinto-do-Ó P. Sca-1(+) Cardiac Progenitor Cells and Heart-Making: A Critical Synopsis. [Internet]. *Stem Cells Dev*. [published online ahead of print: July 14, 2014]; doi:10.1089/scd.2014.0197

11. Segers VFM, Lee RT. Stem-cell therapy for cardiac disease. [Internet]. *Nature*. 2008;451(7181):937–42.

12. Ikram S, Beache GM, Wagner SG, Leri A. Cardiomyopathy : Initial Results of the SCIPIO Trial2013;378(9806):1847–1857.

13. Malliaras K et al. Intracoronary cardiosphere-derived cells after myocardial infarction: evidence of therapeutic regeneration in the final 1-year results of the CADUCEUS trial (CArdiosphere-Derived aUtologous stem CElls to reverse ventricUlar dySfunction). [Internet]. *J Am Coll Cardiol*. 2014;63(2):110–22.

14. Bely AE, Nyberg KG. Evolution of animal regeneration: re-emergence of a field. [Internet]. *Trends Ecol Evol*. 2010;25(3):161–70.

15. Stocum DL. Regenerative biology and medicine. [Internet]. *J Musculoskelet Neuronal Interact*. 2002;2(3):270–3.

16. Sánchez Alvarado A, Tsonis P a. Bridging the regeneration gap: genetic insights from diverse animal models. [Internet]. *Nat Rev Genet*. 2006;7(11):873–84.

17. Ferguson MWJ, O'Kane S. Scar-free healing: from embryonic mechanisms to adult therapeutic intervention. [Internet]. *Philos Trans R Soc Lond B Biol Sci*. 2004;359(1445):839–50.

18. Morgan TH. Experimental studies of the regeneration of Planaria maculata [Internet]. *Arch für Entwickelungsmechanik der Org*. 1898;7(2-3):364–397.

19. Poss K, Wilson L, Keating M. Heart Regeneration in Zebrafish. *Science (80-)*. 2002;298:2188–2190.

20. Jopling C et al. Zebrafish heart regeneration occurs by cardiomyocyte dedifferentiation and proliferation. [Internet]. *Nature*. 2010;464(7288):606–9.

21. Schnabel K, Wu C-C, Kurth T, Weidinger G. Regeneration of cryoinjury induced necrotic heart lesions in zebrafish is associated with epicardial activation and cardiomyocyte proliferation. [Internet]. *PLoS One*. 2011;6(4):e18503.

22. Wang J et al. The regenerative capacity of zebrafish reverses cardiac failure caused by genetic cardiomyocyte depletion. [Internet]. *Development*. 2011;138(16):3421–30.

23. Flink IL. Cell cycle reentry of ventricular and atrial cardiomyocytes and cells within the epicardium following amputation of the ventricular apex in the axolotl, Amblystoma mexicanum: confocal microscopic immunofluorescent image analysis of bromodeoxyuridine-label [Internet]. *Anat Embryol (Berl)*. 2002;205(3):235–44.

24. Laube F, Heister M, Scholz C, Borchardt T, Braun T. Re-programming of newt cardiomyocytes is induced by tissue regeneration. [Internet]. *J Cell Sci*. 2006;119(Pt 22):4719–29.

25. Porrello ER et al. Transient regenerative potential of the neonatal mouse heart. [Internet]. *Science (80-)*. 2011;331:1078–80.

26. Porrello ER et al. Regulation of neonatal and adult mammalian heart regeneration by the miR-15 family. *Proc Natl Acad Sci*. 2013;110(1):187–192.

27. Jesty SA et al. in the neonatal , but not adult , heart. *Proc Natl Acad Sci*. 2012;109(33):13380–13385.

28. Haubner BJ et al. Complete cardiac regeneration in a mouse model of myocardial infarction. [Internet]. *Aging (Albany NY)*. 2012;4(12):966–77.

29. Porrello ER et al. MiR-15 family regulates postnatal mitotic arrest of cardiomyocytes. *Circ Res*. 2011;109:670–679.

30. Soonpaa MH, Kim KK, Pajak L, Franklin M, Field LJ. Cardiomyocyte DNA synthesis and binucleation during murine development [Internet]1996;271(5):H2183–H2189.

31. Aurora AB et al. Macrophages are required for neonatal heart regeneration. *J Clin Invest*. 2014;124(3). doi:10.1172/JCI72181DS1

32. Andersen DC, Ganesalingam S, Jensen CH, Sheikh SP. Do Neonatal Mouse Hearts Regenerate following Heart Apex Resection? [Internet]. *Stem cell reports*. 2014;2(4):406–13.

33. Souders CA, Bowers SLK, Baudino TA. Cardiac Fibroblasts: the renaissance cell. *Circ Res*. 2009;105:1164–1176.

34. Banerjee I, Fuseler JW, Price RL, Borg TK, Baudino T a. Determination of cell types and numbers during cardiac development in the neonatal and adult rat and mouse. [Internet]. *Am J Physiol Hear Circ Physiol*. 2007;293(3):H1883–91.

35. Zak R. Cell proliferation during cardiac growth. [Internet]. *Am J Cardiol*. 1973;31(2):211–9.

36. Ieda M et al. Cardiac Fibroblasts Regulate Myocardial Proliferation through B1 Integrin Signaling. *Dev Cell*. 2009;16(2):233–244.

37. Brown RD, Ambler SK, Mitchell MD, Long CS. The cardiac fibroblast: therapeutic target in myocardial remodeling and failure. [Internet]. *Annu Rev Pharmacol Toxicol*. 2005;45(1):657–87.

38. Crow MT, Mani K, Nam Y-J, Kitsis RN. The mitochondrial death pathway and cardiac myocyte apoptosis. [Internet]. *Circ Res*. 2004;95(10):957–70.

39. Yang F et al. Myocardial infarction and cardiac remodelling in mice Translation and Integration Experimental Physiology : We established a mouse model of cardiac dysfunction due to myocardial infarction (MI). For this we ligated the Experimental Physiology : *Exp Physiol Transl Integr*. 2002;87(5):547–555.

40. Sun Y, Weber KT. RAS and connective tissue in the heart [Internet]. *Int J Biochem Cell Biol*. 2003;35(6):919–931.

41. Baudino T a, Carver W, Giles W, Borg TK. Cardiac fibroblasts: friend or foe? [Internet]. *Am J Physiol Heart Circ Physiol*. 2006;291(3):H1015–26.

42. Lopez B et al. Biochemical Assessment of Myocardial Fibrosis in Hypertensive Heart Disease [Internet]. *Hypertension*. 2001;38(5):1222–1226.

43. Krenning G, Zeisberg EM, Kalluri R. The Origin of Fibroblasts and Mechanism of Cardiac Fibrosis. *J Cell Physiol*. 2010;225(3):631–637.

44. Strutz F et al. Identification and characterization of a fibroblast marker: FSP1. [Internet]. *J Cell Biol*. 1995;130(2):393–405.

45. Kern CB et al. Immunolocalization of chick periostin protein in the developing heart. [Internet]. *Anat Rec Part A*. 2005;284(1):415–23.

46. Goldsmith EC et al. Organization of fibroblasts in the heart [Internet]. *Dev Dyn*. 2004;230(4):787–94.

47. Acharya A et al. The bHLH transcription factor Tcf21 is required for lineage-specific EMT of cardiac fibroblast progenitors. [Internet]. *Development*. 2012;139(12):2139–49.

48. Hudon-David F, Bouzeghrane F, Couture P, Thibault G. Thy-1 expression by cardiac fibroblasts: lack of association with myofibroblast contractile markers [Internet]. *J Mol Cell Cardiol*. 2007;42(5):991–1000.

49. Kruegel J, Miosge N. Basement membrane components are key players in specialized extracellular matrices. [Internet]. *Cell Mol Life Sci*. 2010;67(17):2879–95.

50. Korpos E, Wu C, Sorokin L. Multiple roles of the extracellular matrix in inflammation. [Internet]. *Curr Pharm Des*. 2009;15(12):1349–57.

51. Miyamoto S et al. Integrin Function : Molecular Hierarchies of Cytoskeletal and Signaling Molecules. *J Cell Biol*. 1995;131(3):791–805.

52. Martino MM et al. Engineering the growth factor microenvironment with fibronectin domains to promote wound and bone tissue healing. [Internet]. *Sci Transl Med*. 2011;3(100):100ra89.

53. Hubmacher D, Apte S. The biology of the extracellular matrix : novel insights. *Curr Opin Rheumatol*. 2013;25(1):65–70.

54. Bowers SLK, Banerjee I, Baudino T a. The extracellular matrix: at the center of it all. [Internet]. *J Mol Cell Cardiol*. 2010;48(3):474–82.

55. Corda S, Samuel JL, Rappaport L. Extracellular matrix and growth factors during heart growth. [Internet]. *Heart Fail Rev*. 2000;5(2):119–30.

56. Jung JP, Squirrell JM, Lyons GE, Eliceiri KW. Imaging cardiac extracellular matrices: a blueprint for regeneration. *Trends Biotechnol*. 2012;30(4):233–240.

57. Jacot JG, Martin JC, Hunt DL. Mechanobiology of cardiomyocyte development. [Internet]. *J Biomech*. 2010;43(1):93–8.

58. Gazoti Debessa CR, Mesiano Maifrino LB, Rodrigues de Souza R. Age related changes of the collagen network of the human heart. [Internet]. *Mech Ageing Dev*. 2001;122(10):1049–58.

59. Burgess ML, McCrea JC, Hedrick HL. Age-associated changes in cardiac matrix and integrins. [Internet]. *Mech Ageing Dev*. 2001;122(15):1739–56.

60. Wang J, Karra R, Dickson AL, Poss KD. Fibronectin is deposited by injury-activated epicardial cells and is necessary for zebrafish heart regeneration [Internet]. *Dev Biol*. 2013;382(2):427–35.

61. Chablais F, Jazwinska A. The regenerative capacity of the zebrafish heart is dependent on TGFβ signaling. [Internet]. *Development*. 2012;139(11):1921–30.

62. Mercer S, Odelberg SJ, Simon H-G. A Dynamic Spatiotemporal Extracellular Matrix Facilitates Epicardial-Mediated Vertebrate Heart Regeneration. [Internet]. *Dev Biol*. 2013;:1–15.

63. Lu QL, Partridge T a. A New Blocking Method for Application of Murine Monoclonal Antibody to Mouse Tissue Sections [Internet]. *J Histochem Cytochem*. 1998;46(8):977–983.

64. Freire AG et al. Stable phenotype and function of immortalized Lin-Sca-1+ cardiac progenitor cells in long-term culture: a step closer to standardization. [Internet]. *Stem Cells Dev*. 2014;23(9):1012–26.

65. Chong JJH et al. Adult cardiac-resident MSC-like stem cells with a proepicardial origin. [Internet]. *Cell Stem Cell*. 2011;9(6):527–40.

66. Bollini S et al. Re-activated adult epicardial progenitor cells are a heterogeneous population molecularly distinct from their embryonic counterparts. *Stem Cells Dev*. 2014;23(15):1719–1730.

67. Ponta H, Sherman L, Herrlich P a. CD44: from adhesion molecules to signalling regulators. [Internet]. *Nat Rev Mol Cell Biol*. 2003;4(1):33–45.

68. Midgley AC et al. Transforming growth factor-β1 (TGF-β1)-stimulated fibroblast to myofibroblast differentiation is mediated by hyaluronan (HA)-facilitated epidermal growth factor receptor (EGFR) and CD44 co-localization in lipid rafts. [Internet]. *J Biol Chem*. 2013;288(21):14824–38.

69. Li Y et al. Severe lung fibrosis requires an invasive fibroblast phenotype regulated by hyaluronan and CD44. [Internet]. *J Exp Med*. 2011;208(7):1459–71.

70. Proteoglycan S et al. Fibroblast Invasive Migration into Fibronectin / Fibrin Gels Requires a Previously Uncharacterized Dermatan2004;:266–277.

71. Smith C, Baek S, Sung C, Tallquist M. Epicardial-derived cell epithelial-to-mesenchymal transition and fate specification require PDGF receptor signaling [Internet]. *Circ Res*. 2011;108(12):e15–e26.

72. Alwan A et al. *Global status eport on noncommunicable diseases*. 2010:

73. Mathers CD, Loncar D. Projections of global mortality and burden of disease from 2002 to 2030. [Internet]. *PLoS Med*. 2006;3(11):e442.

74. Pankov R, Yamada KM. Fibronectin at a glance [Internet]. *J Cell Sci*. 2002;115(20):3861–3863.

75. Stoffels JMJ, Zhao C, Baron W. Fibronectin in tissue regeneration: timely disassembly of the scaffold is necessary to complete the build. [Internet]. *Cell Mol Life Sci*. 2013;70(22):4243–53.

76. Imanaka-Yoshida K et al. Tenascin-C modulates adhesion of cardiomyocytes to extracellular matrix during tissue remodeling after myocardial infarction. [Internet]. *Lab Invest*. 2001;81(7):1015–24.

77. Matsui Y, Morimoto J, Uede T. Role of matricellular proteins in cardiac tissue remodeling after myocardial infarction. [Internet]. *World J Biol Chem*. 2010;1(5):69–80.

78. Yabluchanskiy A, Chilton RJ, Lindsey ML. Left ventricular remodeling: one small step for the extracellular matrix will translate to a giant leap for the myocardium. [Internet]. *Congest Heart Fail*. 2013;19(4):E5–8.

79. Hesse M, Fleischmann BK, Kotlikoff MI. Concise review: The role of C-kit expressing cells in heart repair at the neonatal and adult stage. [Internet]. *Stem Cells*. 2014;32(7):1701–12.

80. Kakkar R, Lee RT. Intramyocardial Fibroblast - Myocyte Comunication. *Circ Res*. 2010;106(1):47–57.

81. Potts JD, Runyan RB. Epithelial-mesenchymal cell transformation in the embryonic heart can be mediated, in part, by transforming growth factor beta. [Internet]. *Dev Biol*. 1989;134(2):392–401.

82. Goodison S, Urquidi V, Tarin D. CD44 cell adhesion molecules. [Internet]. *Mol Pathol*. 1999;52(4):189–96.

83. Acharya PS et al. Fibroblast migration is mediated by CD44-dependent TGF beta activation. [Internet]. *J Cell Sci*. 2008;121(9):1393–402.

84. Takamiya M, Haider KH, Ashraf M. Identification and characterization of a novel multipotent sub-population of Sca-1^{+} cardiac progenitor cells for myocardial regeneration. [Internet]. *PLoS One*. 2011;6(9):e25265.

85. Tateishi K et al. Clonally amplified cardiac stem cells are regulated by Sca-1 signaling for efficient cardiovascular regeneration. *J Cell Sci*. 2007;120(10):1791–1800.

11. Supplementary Results

0 Days Post-Apex Resection

Masson's Trichrome Staining

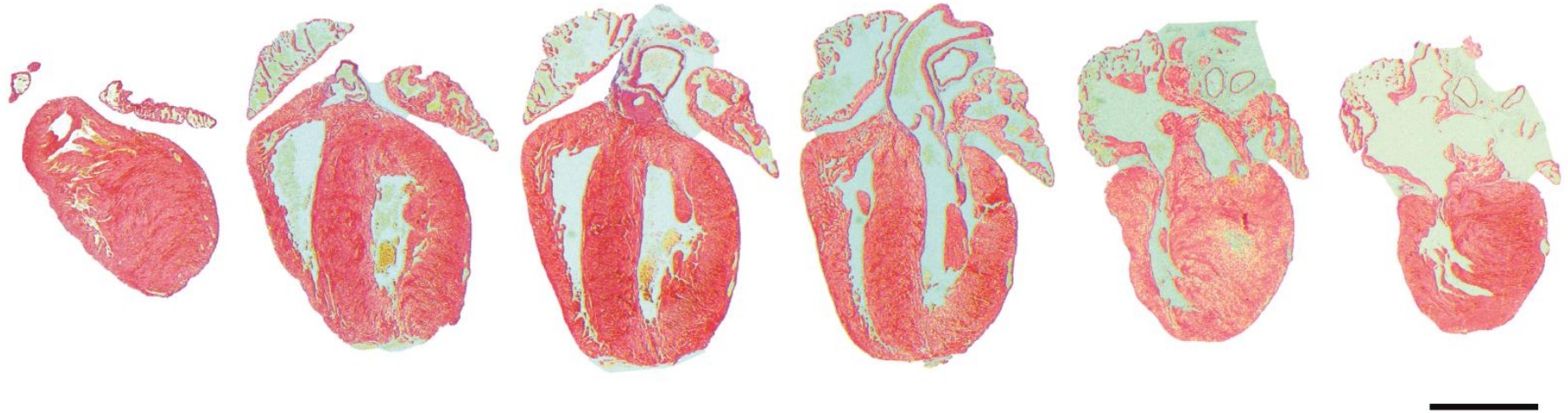

Hematoxylin & Eosin Staining

48 Hours Post-Apex Resection

Masson's Trichrome Staining

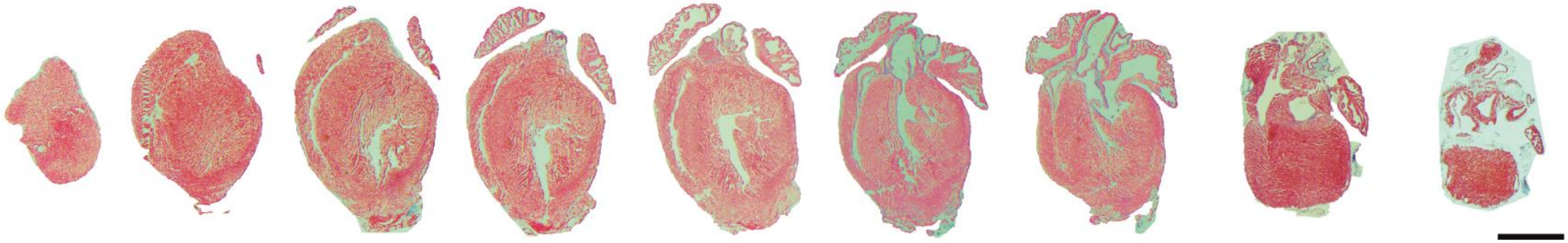

Hematoxylin & Eosin Staining

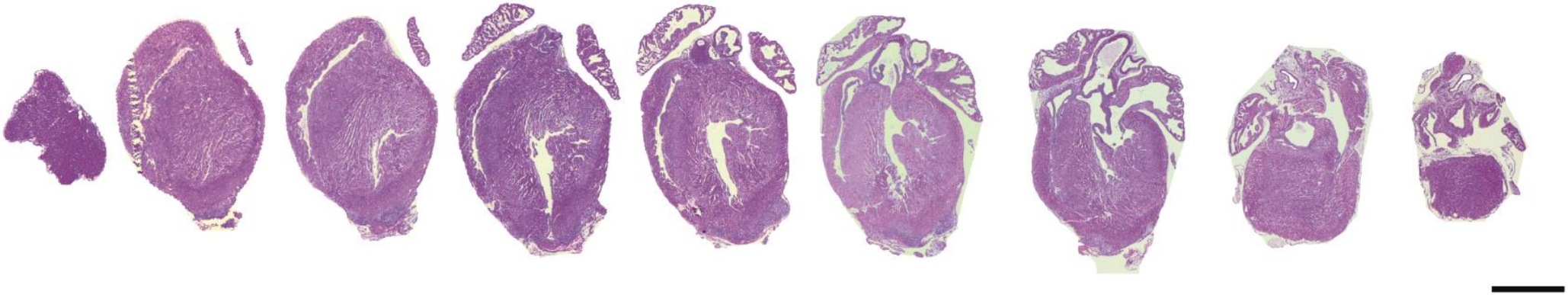

5 Days Post-Apex Resection

Masson's Trichrome Staining

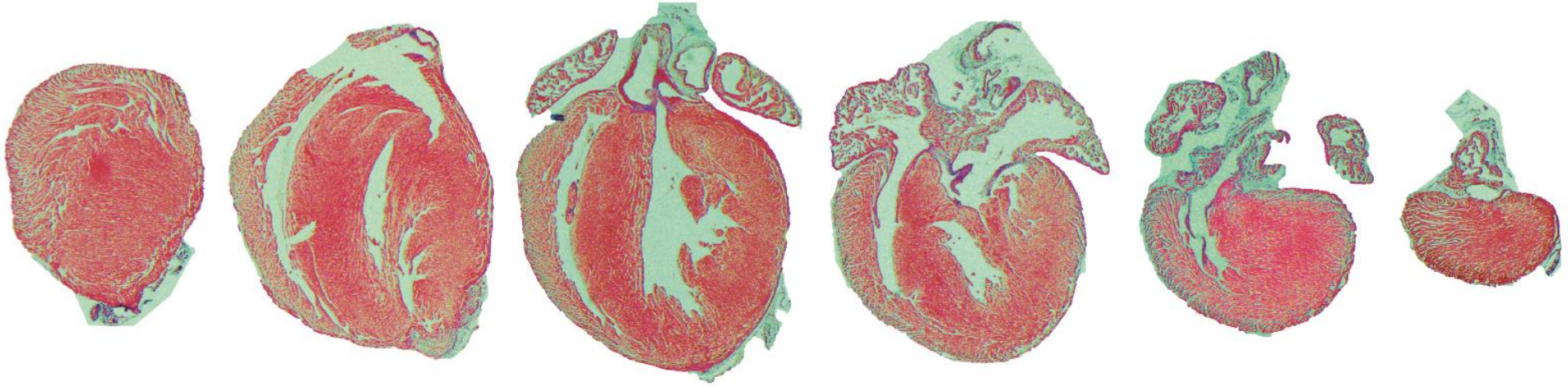

Hematoxylin & Eosin Staining

7 Days Post-Apex Resection

Masson's Trichrome Staining

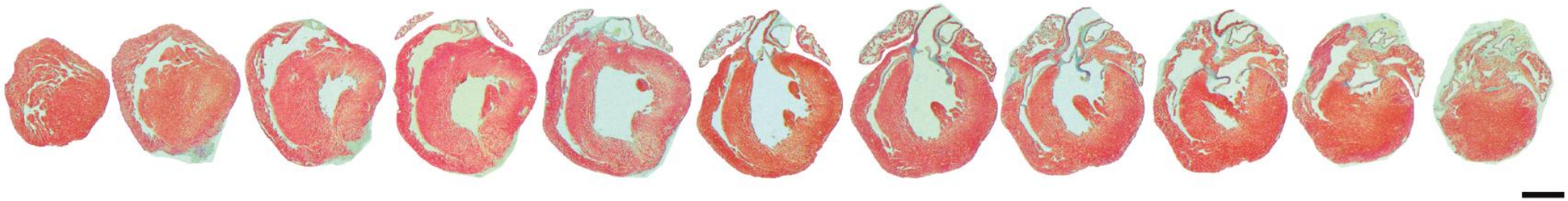

Hematoxylin & Eosin Staining

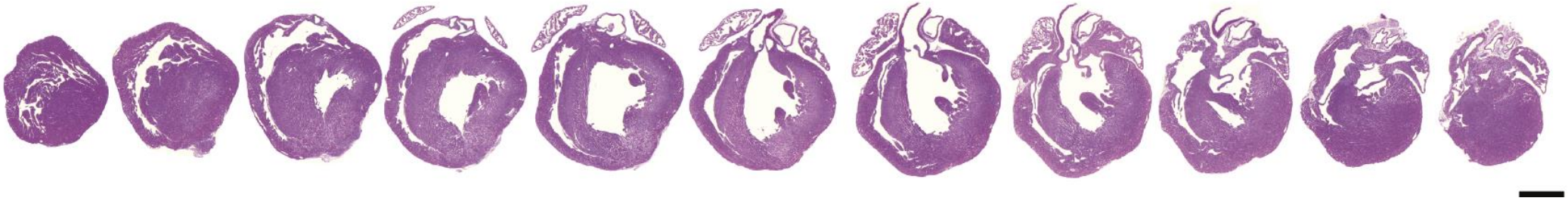

14 Days Post-Apex Resection

Masson's Trichrome Staining

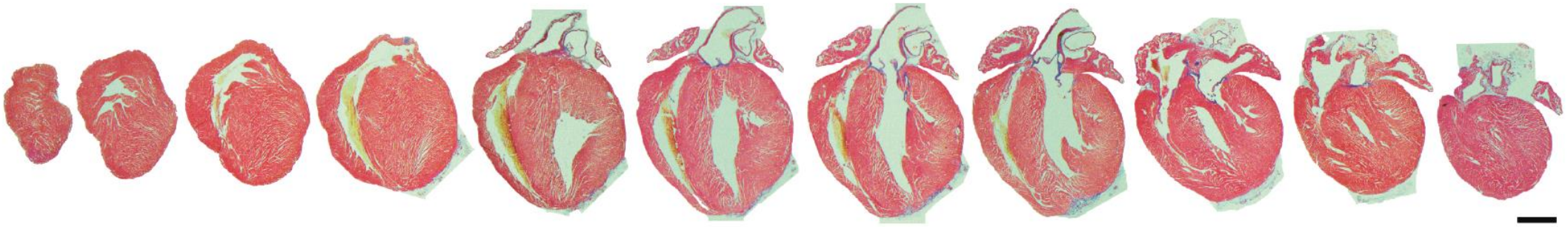

Hematoxylin & Eosin Staining

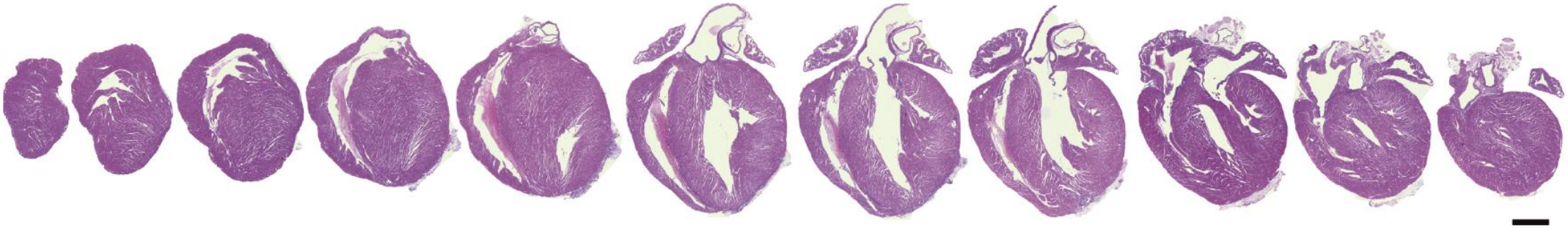

21 Days Post-Apex Resection

Masson's Trichrome Staining

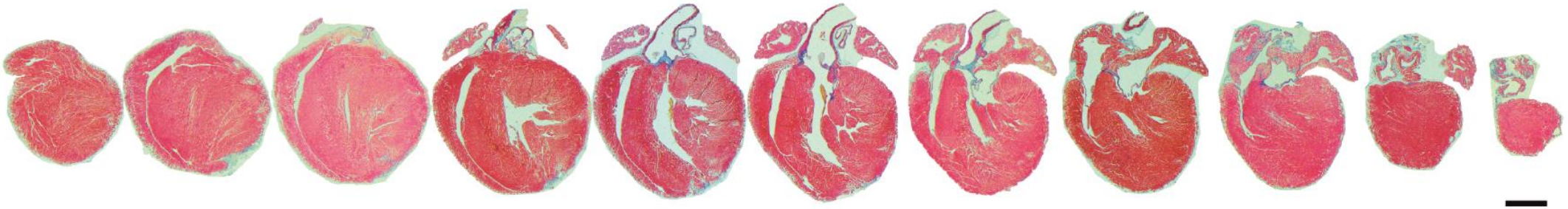

Hematoxylin & Eosin Staining

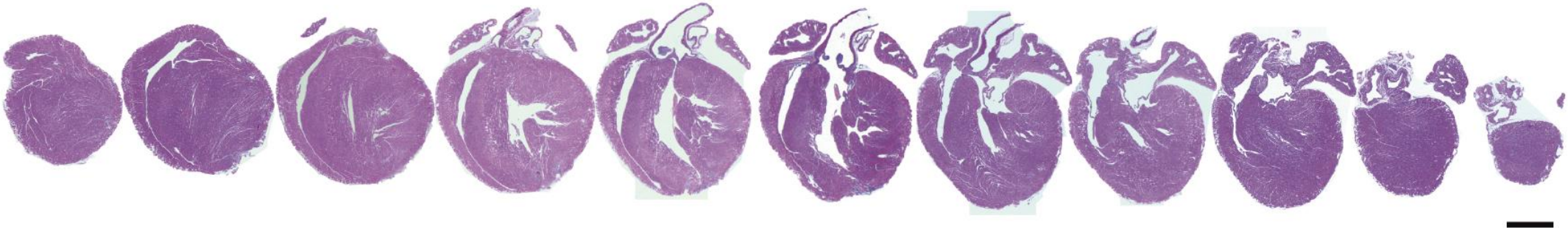

Supplementary Figure 1 – Low power images of Masson's Trichrome and Hematoxilin-Eosin sections of apex-resected hearts at 0, 2, 5, 7, 14, 21 and 60 days post-apex resection surgery (perfomed at P2). These images emphasize the progression of the injury throughout the heart. Representative sampling of the heart was performed by using appropriate spacing between adjacent sections, which vary according to the ontogenic timepoint (see methods). 0, 2, 5, 7, 14 dpr (n=1); 21 dpr (n=4); 60 dpr (n=2). Scale bars: 1 mm (0, 2, 5, 7, 14, 21 dpr), 2 mm (60 dpr).

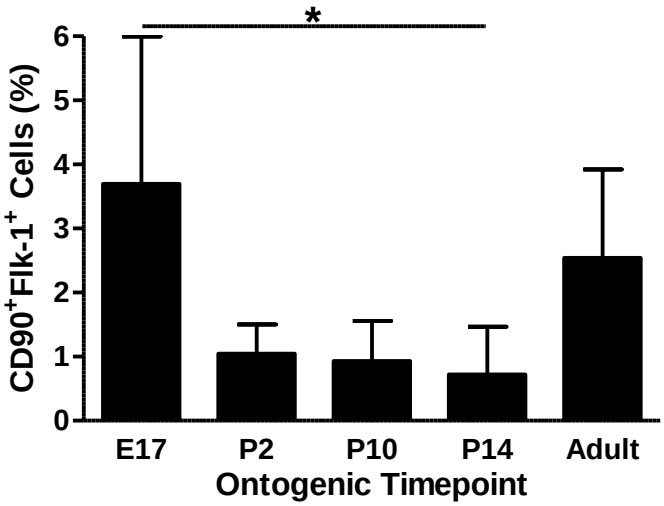

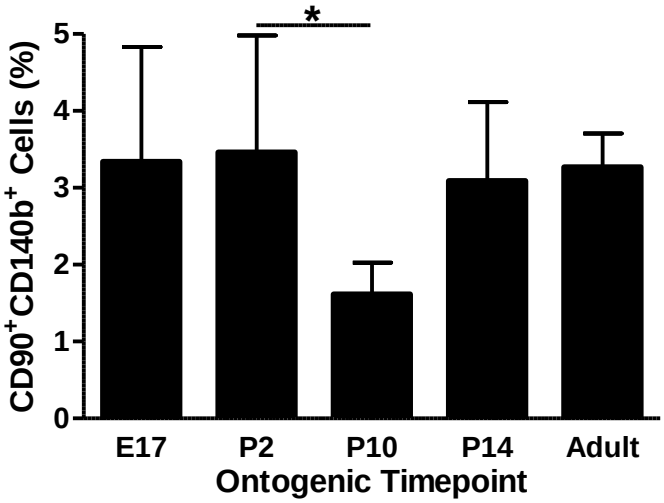

*Supplementary Figure 2 – Flk-1 and CD140b expression profile of CD90 expressing cells troughout ontogeny. E17 (n=6); P2 (n=11); P10 (n=11); P14 (n=11); Adult (n=4). * (p-value < 0,05).*

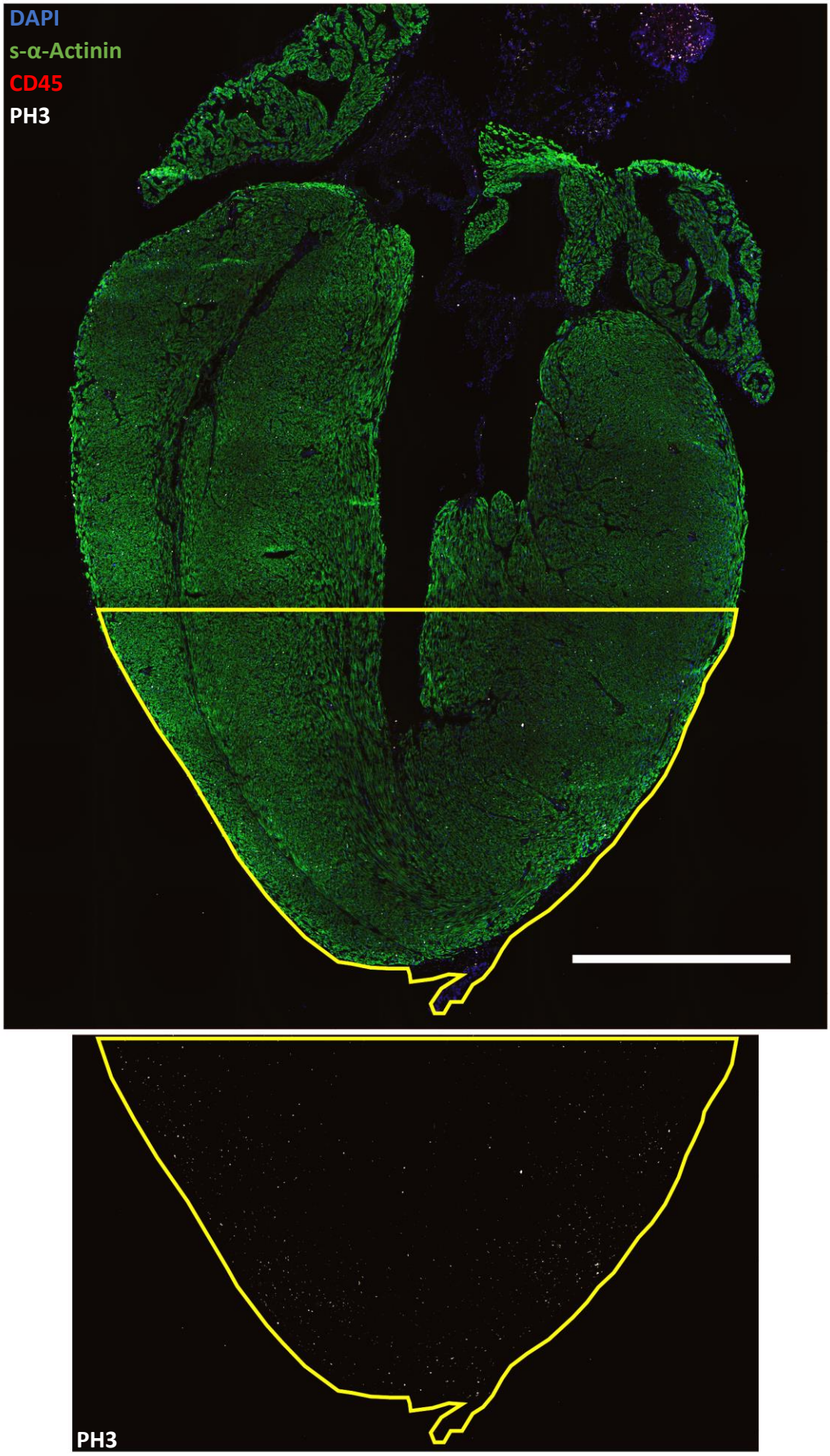

Supplementary Figure 3 – *Co-localization of DAPI, s-α-Actinin, CD45 and PH3 in a representative section of the 7 dpr heart. Quantification of mitotic cells in the apex was performed considering the region between the papillary muscles and the apex (yellow highlight). Isolation of PH3 staining allows the detection of a proliferative gradient (more proliferation in the distal than in the proximal myocardium).Scale-bar, 1000µm.*

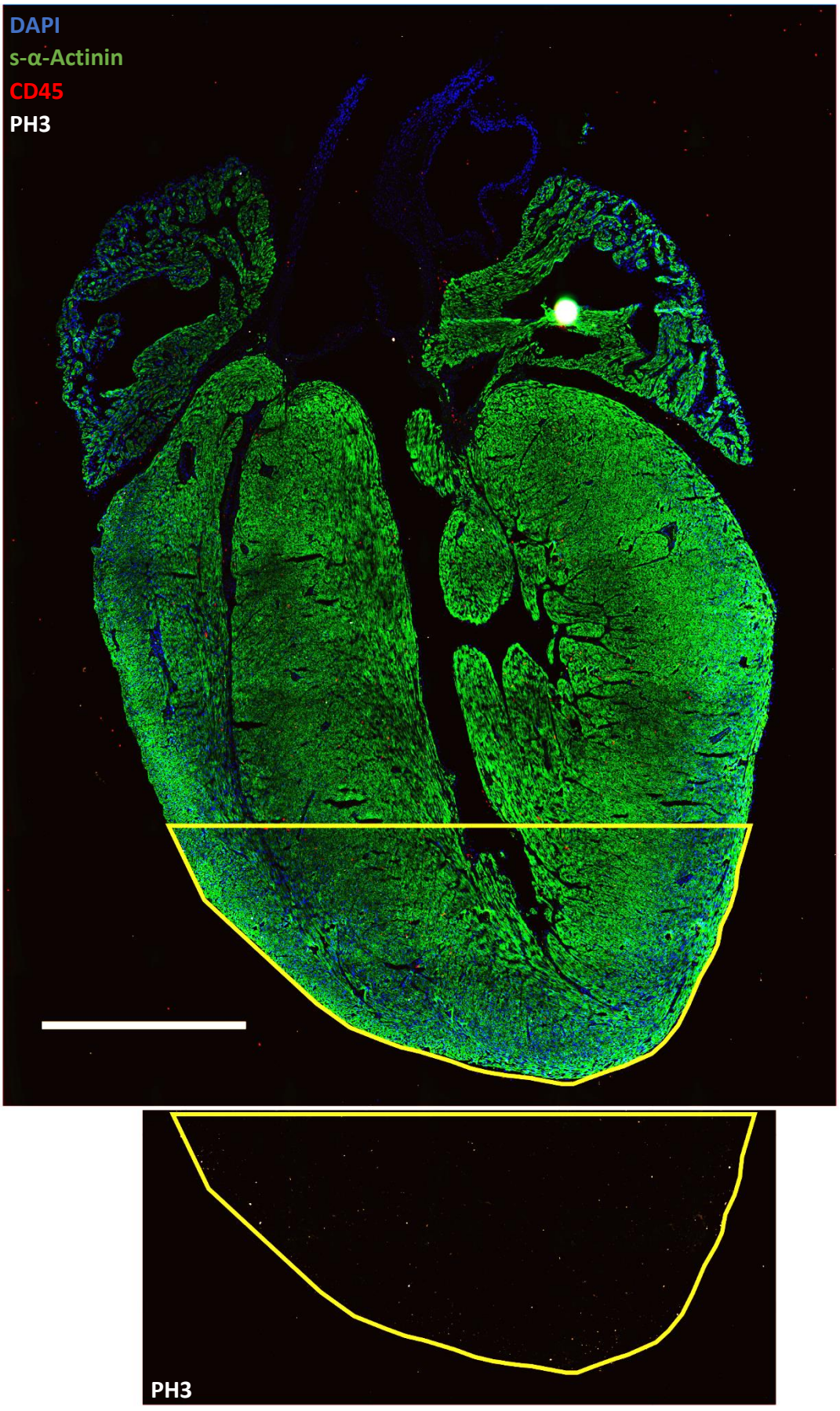

Supplementary Figure 4 – *Co-localization of DAPI, s-α-Actinin, CD45 and PH3 in a representative section of the 7 dps heart. Quantification of mitotic cells in the apex was performed considering the region between the papillary muscles and the apex (yellow highlight). Comparing to 7 dpr, the isolation of PH3 staining does not have a proximo-distal gradient and the number of mitotic cells is decreased. Scale-bar, 1000µm.*